BENZOTRIAZOLE AND QUINOXALINE CONTAINING RANDOM COPOLYMERS FOR BULK-HETEROJUNCTION POLYMER SOLAR CELL APPLICATIONS

A THESIS SUBMITTED TO
THE GRADUATE SCHOOL OF NATURAL AND APPLIED SCIENCES
OF
MIDDLE EAST TECHNICAL UNIVERSITY

BY

CANSEL TEMIZ

IN PARTIAL FULFILLMENT OF THE REQUIREMENTS
FOR
THE DEGREE OF MASTER OF SCIENCE
IN
POLYMER SCIENCE AND TECHNOLOGY

SEPTEMBER 2015

Approval of the thesis:

BENZOTRIAZOLE AND QUINOXALINE CONTAINING RANDOM COPOLYMERS FOR BULK-HETEROJUNCTION POLYMER SOLAR CELL APPLICATIONS

submitted by **CANSEL TEMIZ** in partial fulfillment of the requirements for the degree of **Master of Science in Polymer Science and Technology Department, Middle East Technical University** by,

Prof. Dr. Gülbin Dural Ünver _____
Dean, Graduate School of **Natural and Applied Sciences**

Prof. Dr. Necati Özkan _____
Head of Department, **Polymer Science and Technology**

Assoc. Prof. Dr. Ali Çırpan _____
Supervisor, **Department of Chemistry, METU**

Assoc. Prof. Dr. H. Emrah Ünalan _____
Co-supervisor, **Dept. of Metallurgical and Materials Eng., METU**

Examining Committee Members:

Prof. Dr. Levent Toppare _____
Chemistry Dept., METU

Assoc. Prof. Dr. Ali Çırpan _____
Chemistry Dept., METU

Assoc. Prof. Dr. H. Emrah Ünalan _____
Metallurgical ad Materials Engineering Dept., METU

Assoc. Prof. Dr. Yasemin Arslan Udum _____
Advanced Technologies, Gazi University

Assoc. Prof. Dr. Gülay Ertaş _____
Chem. Dept., METU

Date: 11/09/2015

I hereby declare that all information in this document has been obtained and presented in accordance with academic rules and ethical conduct. I also declare that, as required by these rules and conduct, I have fully cited and referenced all material and results that are not original to this work.

Name, Last name: Cansel Temiz

Signature:

ABSTRACT

BENZOTRIAZOLE AND QUINOXALINE CONTAINING RANDOM COPOLYMERS FOR BULK-HETEROJUNCTION POLYMER SOLAR CELL APPLICATIONS

Temiz, Cansel

M. S., Polymer Science and Technology Department

Supervisor : Assoc.Prof. Dr. Ali Çırpan

Co-Supervisor : Assoc.Prof. Dr. H. Emrah Ünalan

September 2015, 84 pages

In this study, benzotriazole and quinoxaline derivates bearing donor acceptor type three random copolymers were synthesized to achieve broad absorption spectrum in visible region. Quinoxalines are used as strong acceptors in conjugated polymers due to the imine nitrogen in the structure. Quinoxaline containing polymers are green in their neutral states and they reveal two distinct λ_{max} at around 400 and 700 nm. Additionally, benzotriazole and thiophene bearing polymers are red in their neutral states with λ_{max} at around 500 nm. In this manner, quinoxaline derivates were combined with benzotriazole and π-bridge thiophene moieties. 5,8-Dibromo-2,3-di(thiophen-2-yl)quinoxaline, 5,8-dibromo-2,3-diphenylquinoxaline and 10,13-dibromodibenzo[a,c]phenazine acceptor units were united with 4,7-dibromo-2-(2-octyldodecyl)-2H-benzo[d][1,2,3]triazole and 2,5-bis(trimethylstannyl)thiophene via Stille coupling reaction to yield alternating donor acceptor parts with randomly

distributed several different acceptor units through polymer backbones with broad absorption in visible region. Synthesized polymers were characterized with NMR, thermogravimetric analysis, cyclic voltammetry and UV-Vis-NIR spectroscopy. Organic solar cells device production and current-voltage property measurements were conducted in a nitrogen-filled glove box system. Organic solar cell devices with the configuration of ITO/PEDOT:PSS/Polymer:$PC_{71}BM$/LiF/Al were fabricated in which polymers serve as electron donors and $PC_{71}BM$ as the electron acceptor in the active layer. Power conversion efficiencies of Polymer: $PC_{71}BM$ blends were measured under standard AM 1.5 G illumination (100 mW/cm^2). The organic solar cells devices employing **CoP1**:$PC_{71}BM$ films showed power conversion efficiencies up to 2.13%.

Keywords: Benzotriazole, quinoxaline, conjugated polymers, electrochemistry, organic solar cell

ÖZ

YIĞIN HETEROBAĞLANTILI BENZOTRİAZOL VE KİNOKSALİN İÇEREN RASTGELE KOPOLİMERLERİN POLİMER GÜNEŞ HÜCRESİ UYGULAMALARI

Temiz, Cansel

Yüksek Lisans, Polimer Bilimi ve Teknolojisi Bölümü

Tez Yöneticisi : Doç.Dr. Ali Çırpan

Ortak Tez Yöneticisi : Doç.Dr. Emrah Ünalan

Eylül 2015, 84 sayfa

Bu çalışmada benzotriazol ve kinoksalin türevleri içeren donor-akseptör tipi üç kopolimer görünür bölgede geniş soğurma elde etmek amacıyla sentezlenmiş ve organik fotovoltaik hücre performansları yığın heterobağlantılı organik güneş hücrelerinde ölçülmüştür. İçerisindeki imin sayesinde kinokzalin yapıları π-konjuge polimeler yapılarında güçlü bir akseptör görevi görmektedir. Kinoksalin içeren polimerler nötral hallerinde yeşil renk sahip olmakla beraber 400 nm ve 700 nm'de iki λ_{max} göstermektedir. Buna ek olarak, benzotriazol ve tiyofen yapıları barındıran polimerler nötral hallerinde 500 nm'deki λ_{max} ile kırmızı renk göstermektedir. Bu özellikler göz önünde bulundurarak, çalışmada bu yapıların birleştirilmesiyle görünür bölgede geniş soğurma amaçlanmıştır. Farklı akseptör ünitlerine sahip rastgele dağılımlı donor-akseptör tipi kopolimerler elde etmek amacıyla 5,8-dibromo-2,3-di(tiyofen-2-yl)kinoksalin, 5,8-dibromo-2,3-difenilkinoksalin ve 10,13-dibromodibenzo[a,c]fenazin akseptör yapıları 4,7-dibromo-2-(2-oktildodesil)-2H-

benzo[d][1,2,3]triazol ve 2,5-bis(trimetilstanil)tiyofen üniteleri ile Stille kenetlenme reaksiyon ile birleştirilmiştir. Sentezlenen polimerler NMR, ısıl ağırlık ölçümsel analizleri, dönüşümlü voltametri ve UV-Vis-NIR bölge spektroskopi ile karakterize edilmiştir. Organik güneş pili cihaz yapımı ve akım-voltaj ölçümleri eldivenli kabin sisteminde yürütülmüştür. Aktif bölgesinde polimerlerin elektron donör ve $PC_{71}BM$'in elektron alıcı olarak kullanıldığı organik güneş pili yapımı ITO/PEDOT:PSS/Polymer:$PC_{71}BM$/LiF/Al konfigürasyonunda gerçekleştirilmiştir. Polimer:$PC_{71}BM$ karışımlarının güç dönüşüm verimleri standart AM 1.5 G aydınlatması ile (100mW/cm^2) ölçülmüştür. **CoP1**:$PC_{71}BM$ film kullanılan organik güneş hücreleri 2.13% güç dönüşüm verimi göstermiştir.

Anahtar Kelimeler: Benzotriazol, kinoksalin, konjüge polimerler, elektrokimya, organik güneş pili

To my dear family

ACKNOWLEDGMENTS

Firstly, I would like to express my sincere gratitude to my supervisor Assoc. Prof. Dr. Ali Çırpan for his continuous support of my thesis study, his endless patience and invaluable guidance. Although I graduated, I am aware of that he will remain as an advisor for me during my whole life. I couldn't have imagined having a better advisor than him for my MSc study.

I would like to thank my co-adviser Assoc. Prof. Dr. H. Emrah Ünalan for his guidance, infinite support and important advices according to my thesis study.

Besides my advisor, I would like to thank Prof. Dr. Levent Toppare for his diligent guidance, support, encouragement and especially for his confidence in me. During meetings, his questions and comments were very beneficial to gain an excellent academic perspective. I have learnt a lot from his insight.

Any words are enough to express my gratitude to Şevki Can Cevher. Since I started to study in Cirpan Research Group, he became more than a mentor. He always compelled me to think deeply in polymer and organic chemistry. I would like to thank him for his endless patience and support during my whole thesis study period. I will never forget our sleepless nights in the laboratory, deep relationship chats and the way we make each other laugh. He deserves the best 'mama cakes' with milk.

I would also thank Dr. Naime Akbaşoğlu Ünlü for her limitless patience, support and precious guidance. Due to her studies in the USA and pregnancy period to my lovely niece Zeynep, we couldn't spend so much time in the laboratory but she was always there for me whenever I needed her.

I would like to express my feelings to Hande Ünay and Ece Aktaş for their amazing friendships, motivations and our joyful gossips and chats during coffee breaks. My two year-long MSc adventure earnt me two lovely friends. Wherever we will go, I ensure you with no doubt, you will remain in my life.

Special thanks to my laboratory mates İpek, Özge, Duygu, Ozan and Emre for their friendships and providing such a peaceful laboratory environment. They made laboratory joyful and I feel so lucky being a part of Cirpan Research Group.

I am grateful to Assoc. Prof. Dr. Yasemin Aslan Udum, Assoc. Prof. Dr. Dilber Esra Yıldız and Gönül Hızalan for their help in electrochemical, mobility and organic solar cell device studies.

I owe a lot to my precious parents, my role model genius brother Dr. Yuksel Temiz and my amazing sister-in-law Selma Gürsel Temiz who encourage and help me in every moment of my personal and academic life. I wouldn't withstand against any crisis and injustice without their wisdom, endless love, support and understanding. It is remarkable to feel your love always by my side.

This thesis is only a beginning of my journey.

TABLE OF CONTENT

LIST OF TABLES

LIST OF FIGURES

LIST OF ABBREVATIONS

CP Conjugated polymer

ECD Electrochromic device

CE Coloration efficiency

OLED Organic light emitting diode

HOMO Highest occupied molecular orbital

LUMO Lowest unoccupied molecular orbital

OFET Organic field effect transistor

PCE Power conversion efficiency

CB Conduction band

VB Valence band

D-A Donor-Acceptor

OSC Organic solar cell

ITO Indium tin oxide

PSS Polystyrenesulfonate

PEDOT Polyethylene dioxythiophene

PCBM [6,6]-Phenyl C 71 butyric acid methyl ester

BHJ Bulk heterojunction

η_e Power conversion efficiency

J_{sc} Short circuit current density

V_{oc} Open circuit voltage

FF Fill factor

P_{max} Maximum power

P_{in} Power of the incident light

R_{sh} Shunt resistor

Rs Series resistor

AM 1.5 G Air mass 1.5 global

CV Cyclic voltammetry

THF Tetrahydrofuran

$TBAPF_6$ Tetrabutylammonium hexafluorophosphate

ACN Acetonitrile

NHE Normal hydrogen electrode

Eg^{op} Optic band gap

TGA Thermal gravimetry analysis

DSC Differential scanning calorimetry

UV Ultraviolet

Vis Visible

NIR Near infrared

ICT Intermolecular charge transfer

IPCE Internal power conversion efficiency

EQE External quantum efficiency

CHAPTER 1

1. INTRODUCTION

1.1. π- Conjugated Polymers

Conjugated system is a structure where molecule contains alternating single and multiple bonds. In such molecules, conjugation can be obtained in two ways. It can be the interaction between one p-orbital and another across a superseding σ-bond. The system can also be achieved by the interaction a p-orbital having an unshared electron pair.[1] Conjugated polymers (CPs) are widely used in academia and industry. The interest in conjugated polymers has begun with the discovery of electrical conductivity of polyacetylene which increases considerably upon electrochemical doping.[2,3] Due to this discovery, three scientists, Alan Heeger, Alan MacDiarmid, and Hideki Shirakawa received the 2000 Nobel Prize in Chemistry.

The invention of electronically conducting polymers has opened new doors for chemistry and physics.[3] Due to their electrical and physical properties, new structural designs of CPs gained traction in the field of energy storage, electrocatalysis, organic electrochemistry, bioelectrochemistry, photoelectrochemistry, sensors, electrochromic displays, etc. Over the last few decades, they appreciably have been used in Organic Light Emitting Diodes (OLEDs), Organic Effect Transistors (OFETs), Organic Solar Cells (OSCs) and Electrochromic Devices (ECDs).[3,4] Especially, conjugated polymers (**Figure 1**) have been

intensively studied in the active layer of ECDs and OSCs due to their processibility, long-term stability, low cost for device fabrication, rapid switching time, and high optical contrast features. Moreover, owing to ease of tuning color via small modifications on the conjugated polymers, CPs have become a major field among researchers. Although many different colored CPs in the neutral state have been studied, achieving black colored polymers is still a desirable challenge due to the necessity of the polymer that absorbs the entire visible region homogeneously.[1-6]

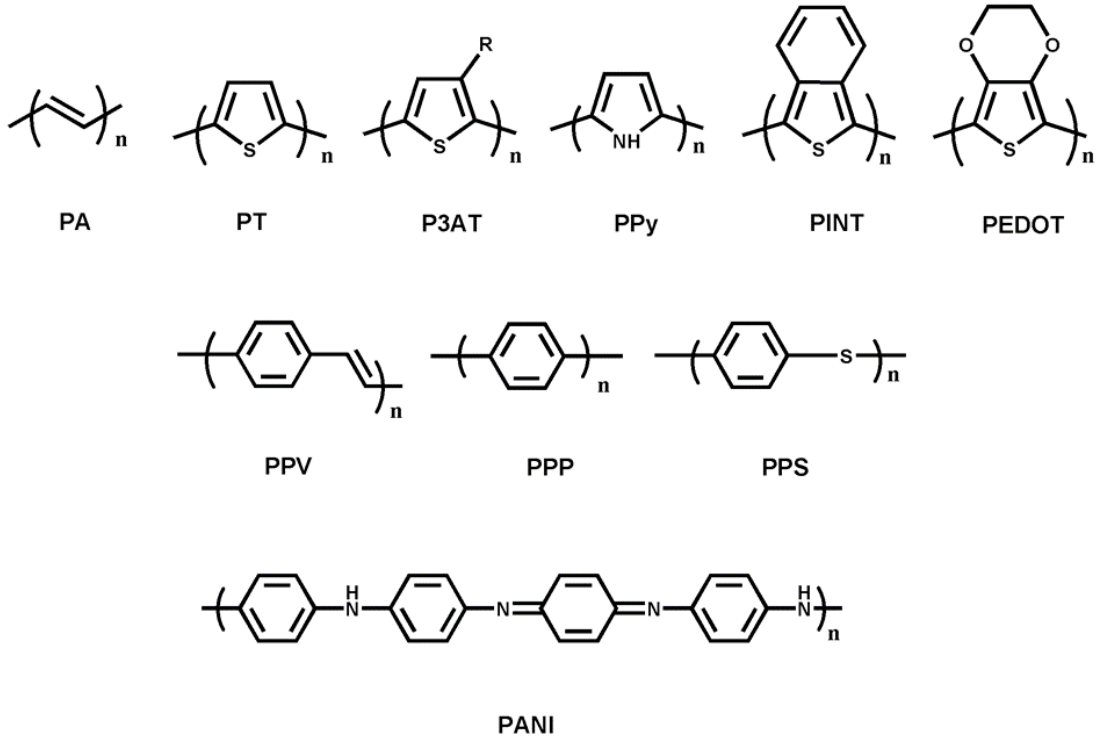

Figure 1. Some examples of widely used CPs

Especially in ECDs and OSCs, conjugated polymers have been used widely due to their conducting properties. However, conjugated polymers are insulators in their neutral state. In order to obtain conducting property, doping process is applied. By electrochemical or chemical doping processes, new electronic states namely polaron and bipolaron bands are obtained. By the help of those new electronic states, conductivity, optical and

optoelectronic properties of polymers are increased. Hence, doping process which is explained in the next section is one of the main parameters for conjugated polymers.

1.1.1. Doping Process

Doping process is achieved in two major ways: chemical doping and electrochemical doping. In electrochemical doping, due to the presence of an electrolyte solution, anion of the electrolyte plays an important role. The basic principle of chemical doping is introducing dopant molecules into an organic semiconductor material by spin casting from solution or by co-evaporation in vacuum.[7] For doping organic semiconductors, there are several conditions to be satisfied. The dopant must be fixed in the semiconductor lattice. In the film, there must be no mobile ions. The dopant must be close enough to host so it will have a tendency to separate from it. And, the oxidation and reduction potentials of dopant must be similar to those of the host that is the dopant does not form a deep electrical trap.[8]

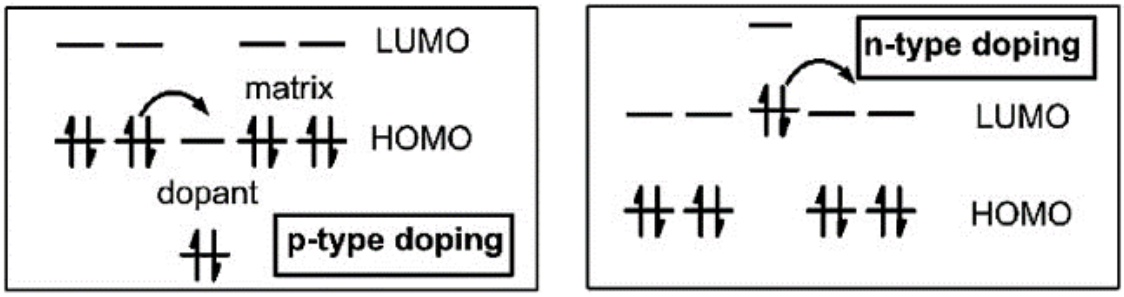

Figure 2. Schematic representation of molecular doping in organic semiconductors p-typed (left) and n-type (right)[9]

Doping process can be used in the controlling of Fermi-level which is related with the number of free charge carriers upon organic semiconductors. Fermi-level position is controlled as the increasing charge carrier density and as conductivity increases, ohmic losses across the active layer is reduced. Moreover, the efficiency of the doping process features in the number of created free charge carriers per dopant molecule. At higher

concentration of dopants, the number of free charges increase hence, the voltage increases.[9] During this process, electron donor and acceptor are added to the material. As illustrated in **Figure 2**, in n-type doping, the dopant which acts as the donor supplies electrons to the lowest unoccupied molecular orbital (LUMO) states and their ionization energy (IE) must be analogous or even lower than the electron affinity (EA) of the host material. Visa versa, in p-type doping, the dopant which acts as the acceptor, has to extract electrons from the highest occupied molecular orbital (HOMO) states to create holes. The electron affinity (EA) of the dopant molecules must be equal or even greater than the ionization energy (IE) of the host molecules.[8,9]

In recent years, scientists are focused on doping of organic semiconductors to be used in organic solar cells. Both n-type and p-typed doped active layers serve some advantages to OSCs. Using doped transport layer with wide-gap, without giving any possibility to shorts or recombination at the active layer- metal interfaces, active layer thickness can be reduced to photovoltaic active volume. Moreover, OSCs are operated at very low voltages. Thus avoiding voltage drops is critical. By doping process, Ohmic contacts can be obtained and voltage drop can be avoided more efficiently.[9]

1.2. Band Theory

Materials are classified according to their electric conductivity as metals, semiconductors and insulators. The electric conductivity is directly related to the band gap. Band gap is defined as the difference between highest occupied molecular orbital (HOMO) and lowest unoccupied molecular orbital (LUMO) or the energy gap between conduction band (CB) and valence band (VB) of the material.[10] Conductivity arises by the movement of the excited electrons from occupied band to unoccupied energy levels thermally or photochemically.

In metals, the band gap is zero due to overlapping of VB and CB of metals.[10-12] VB of conductors is partially filled and it has many empty levels where electron can move by the electric field. In contrast to conductors, in insulators, the band gap between HOMO and

LUMO energy levels is too large resulting from the fully occupied VB and fully empty CB. It makes the movement of the excited electrons almost impossible so they do not have electrical conductivity. Semiconductors take place in between conductors and insulators with their larger band gap than that of conductors and smaller band gap than insulators. VB of semiconductors is almost fully empty and CB is almost completely filled. Therefore, electrons can travel from CB to VB and produce electrical conductivity. The band gap theory of the materials is shown in the **Figure 3.**[13,14]

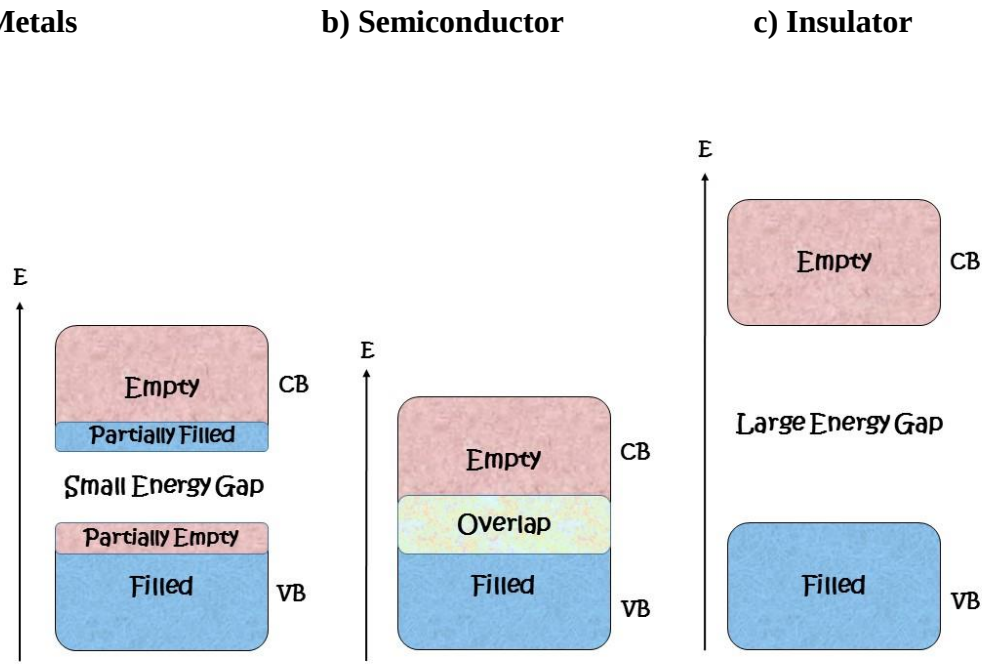

Figure 3. The band gap theory of materials: a) Metals b) Semiconductors c) Insulators

The difference between HOMO and LUMO defines the optical and optoelectronic properties of the π-conjugated polymers. These features can be controlled via several

strategies. This structural alternations also give the opportunity to obtain low band gap conjugated polymers.[15]

1.2.1. Band Gap Engineering

Optical and optoelectronic properties of materials depend on the band gap. Tuning the band gap process is also called band gap engineering and it depends on several parameters. As shown in **Figure 4**, by sum of those parameters (bond length alternation (E_{BLA}), substituents (E_{Sub}), aromaticity (E_{Res}), planarity (E_{θ}) and intermolecular interactions (E_{int})) band gap of conjugated polymers can be determined.[16]

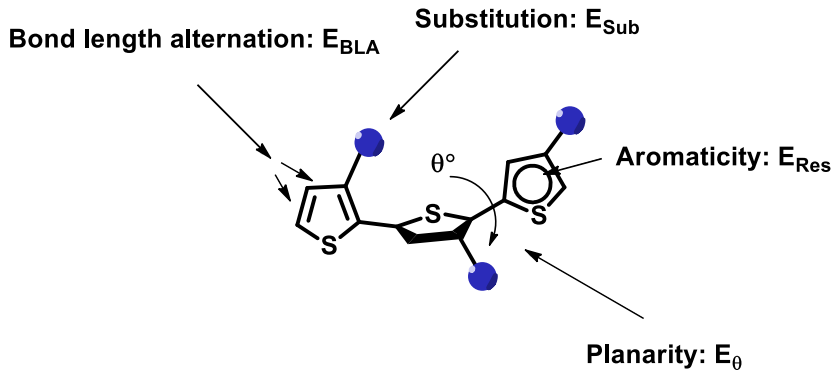

Figure 4. Band gap tuning parameters for conjugated systems[16]

Conjugated polymers are classified with their resonance structures in the ground state: Aromatic and quinoid forms. Bond length alternation (BLA) is the ratio of aromatic to quinoid population in a π-conjugated main chain and by changing this ratio band gap can be lowered. Aromatic form can be converted into quinoid form via π-electron delocalization which decreases the band gap.[16,17] As the aromatic form increases in the conjugated main chain, due to the increase in the BLA band gap also increases. However, if a conjugated polymer is mainly subjected to quinoid form, owing to the rise in the

double bond nature between two neighboring rings (as shown in the **Figure 5**) BLA decreases. As a result, lower band gap is achieved.[17]

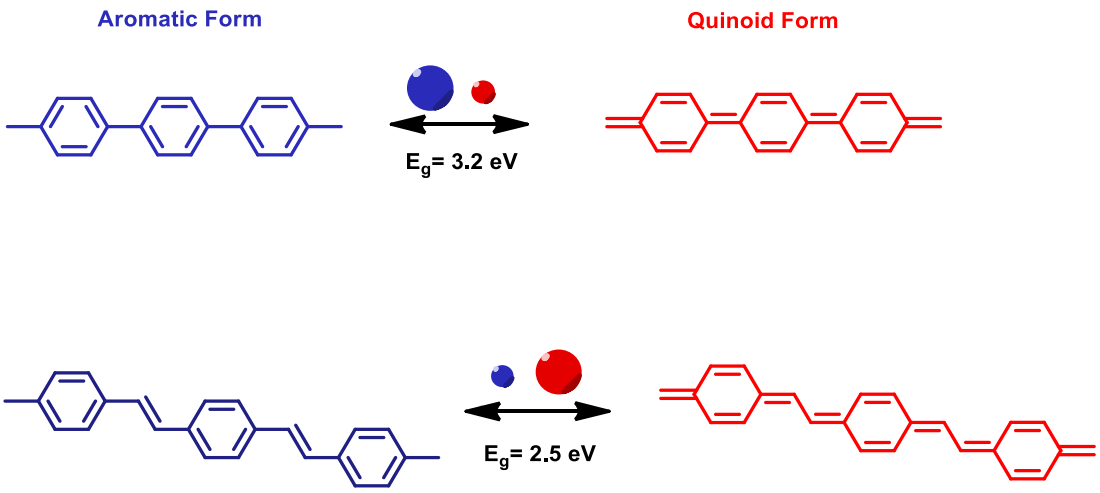

Figure 5. Bond length alternation effect on band gap[17]

Aromaticity restrains the electrons on the ring owing to the π-electron delocalization and it leads electrons be less mobile on the conjugated polymer backbone which results in distortion on the conjugation length. Hence, as the aromaticity increases, the band gap of the conjugated polymers increases.[18]

In π-conjugated polymer backbones, carbon atoms have sp^2p_z hybridization. While each carbon atoms has three σ bonds in the sp^2 form, p_z represents π overlapping with the neighboring p_z orbital.[19] If those p orbitals are perpendicular to each other instead of overlapping, electrons delocalize and conjugation is interrupted. Conjugation length is inversely proportional to energy band gap. More clearly, as conjugation length increases, or planarity decreases, BLA decreases so lower band gap polymers are obtained.[17,18]

Another effective way to achieve suitable band gap is the contribution of different functional groups into the polymer backbone. In general, anchoring electron withdrawing group increases the electron affinity and ionization potential which decreases the LUMO energy level. In contrast, contribution of electron donating group decreases the band gap by increasing the HOMO energy level.[20,21]

Molecule's chemical state affects the band gap as one obtain lower band gap in the solid state than in the solution phase. Solid state provides more ordered crystalline, more rigid structure which increases the intermolecular interactions. This rigid structure also improves the π-π stacking leading to red shift on the ground state spectrum thus lower band gap polymers are achieved.[21,22]

1.3. Donor- Acceptor Approach

In order to tune band gap, structural modification is the keystone for optical and optoelectronic properties of CPs.[23] Recent research shows interest in donor-acceptor (D-A) approach which comprise different type of electron rich (donor) and electron deficient (acceptor) units on the polymer backbone. This can control bond length alternation, electron delocalization and quinoid form formation hereby energy band gap of the polymers. This theory was discovered for the first time by Havinga et al. and they claimed that low band gap polymers can be obtained by combining different types of donor (D) and acceptor (A) moieties.[24,25] In this approach, high HOMO energy level donor and low LUMO energy level acceptor matches and form new low band gap energy.[26] By using D-A approach, Reynolds et al. designed new polymers containing cyanovinylene group as the acceptor unit together with several different donors (**Figure 6**). In this study, effective combination of different donor and acceptor units serves lower band gaps.[27] In this manner, effective selection of donor and acceptor units and careful design of polymers can provide control over band gap, optical and optoelectronic properties.

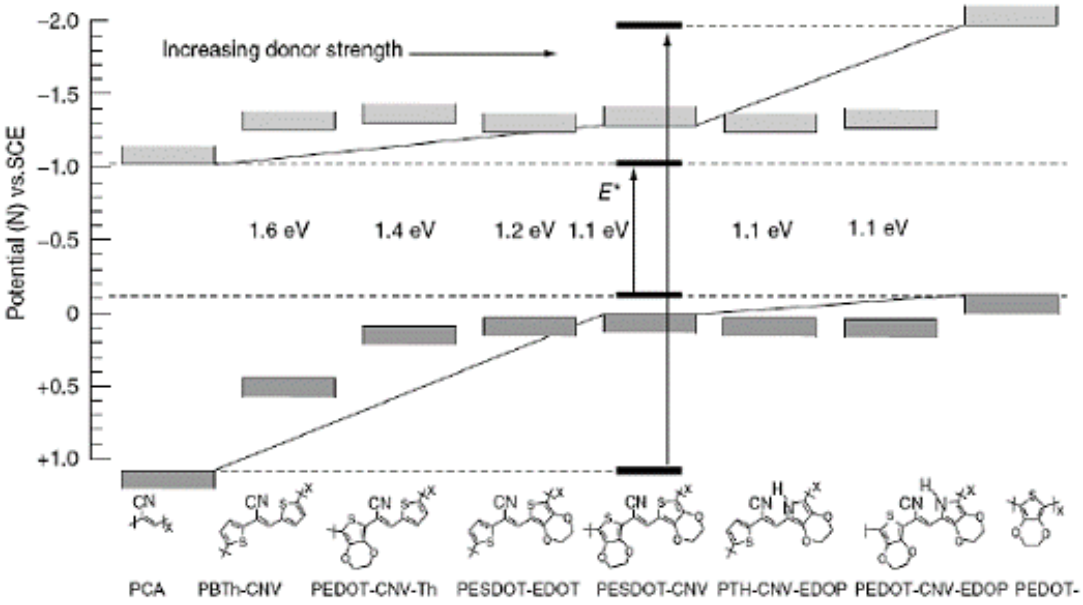

Figure 6. The effect of Donor-Acceptor approach on band gap[27]

1.4. Moieties in Donor-Acceptor Approach Conjugated Polymers

1.4.1. Quinoxaline Moiety

Quinoxalines (benzopyrazine) are the aromatic heterocyles containing benzene fused pyrazine ring in the structure. Due to imine nitrogens in pyrazole ring, quinoxaline derivates are being used as strong acceptor units in low band gap conjugated polymers. Quinoxaline structure can be tailored from 2 and 3 positions to control solubility, electrochemical and photovoltaic properties of D-A type copolymer. Therefore, they have being used in wide application areas mostly in photovoltaics and pharmaceuticals.[28,29]

1.4.2. Benzotriazole Moiety

Benzene fused aromatic heterocycles are called benzazoles which were used as the acceptor units in the synthesis of conjugated polymers via D-A approach due to their unique electrical and optoelectrical properties. Two electron withdrawing imine bonds (C=N) in benzazole structure provide high electron transporting feature.[30] Benzotriazole (BTz) is a class of benzazoles which were utilized as the electron deficient units mostly in optoelectronic and photovoltaic applications. For the first time, BTz bearing conjugated was synthesized by Yamamoto et al and used in optoelectronic applications.[31] Moreover, in 2008, electrochemically polymerized BTz bearing conjugated polymer was firstly designed and synthesized by Toppare et al.[32] Due to trivalent character of nitrogen atom in BTz structure, BTz can be functionalized with alkyl chain to overcome solubility problem. In addition to solubility problem, electron donating feature of alkyl chain can be modified.[33,34]

1.4.3. π-Bridge Group: Thiophene Moiety

Sulfur and selenium are among the group 6 atoms which can form chalcogens. The electron donor π-bridge cyclic molecules have been widely used for the alternating electronic and optical properties of the materials in the donor-acceptor approach. The most widely used heterocyclic conjugated molecule as a π-bridge unit is thiophene. Electron-rich thiophene unit tends to lower aromaticity into a quinoid structure which can reduce the bond alternation energy and polymer band gap energy consequently. Moreover, thiophene rings demonstrate advantages of low lying HOMO energy level and enhanced absorbance. Besides this approach, using thiophene ring as π-bridge group in D-A type polymer backbone, polymer band gap can be reduced by increasing π-conjugation length.[35, 36]

1.5. Electrochromism

Chromism is the reversible color or transmission change upon applied chemical or physical stimuli. According to applied stimulus such as light, heat, solvent, potential, etc., chromism is classified as photochromism, thermochromism, solvatochromism, electrochromism.[37] Electrochromism is the visible and reversible color change upon applied potential via reduction and oxidation reactions. By electrochromism, optical properties of the materials can be examined. During oxidation and reduction processes, by upon applied potential, different electronic absorption bands are generated. Consequently, different colors of the materials in their neutral, reduced, oxidized or intermediate states can be observed. The effect of electrochromism may not only be detected in visible region, but also in ultraviolet (UV) and infrared (IR) regions in electromagnetic spectrum.[38,41]

Electrochromic materials are classified as metal oxide films, viologens and conducting polymers. The most studied electrochromic metal oxide is tungsten trioxide (WO_3). WO_3 is yellow while WO_2 is brown. Electrochromism in WO_3 generates a color change upon electrochemical reduction via adding zinc metal as reducing species. During this process, the color change results from a slight loss of oxygen generating an additional valence state in the parent WO_3. Cation-to-cation charge transfer between parent W6+ and reduced ions are responsible for the color change.[39]

Viologens, a class of molecular dyes, are electrochromic materials due to their chemical structure. Electrochromism in viologens causes by the formation of viologen radical cations via reductive electron transfer as shown in the **Figure 7**. During this process, diquarternization of 4,4’-bipydridyl yields 1,1'-disubstituted- 4,4'-bipyridilium salts. The color of viologens can be colored by the addition of alkyl chains or substituents. For example, methyl group substituted viologens are blue in their radical cation form while they are almost transparent in their neutral or dication form. Moreover, if n-heptyl is

substituted the color becomes purple whereas if p-cyano-phenyl is anchored to viologen, green color is detected.[40,41]

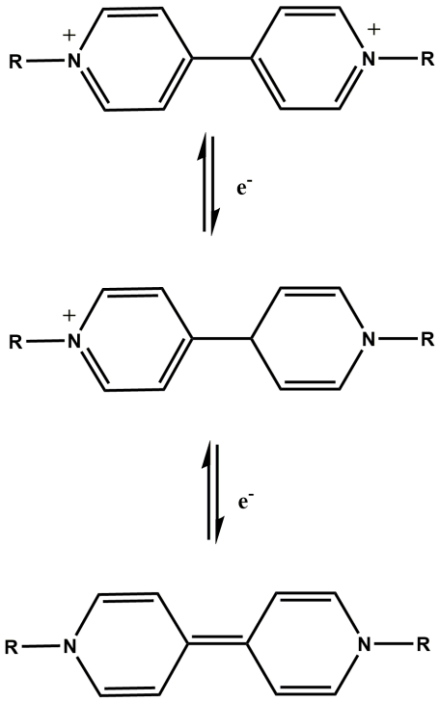

Figure 7. Formation of viologen radical cations via reductive electron transfer[40]

1.5.1. Electrochromism in Conjugated Polymer

Electrochromic conjugated polymers have aroused great attention recently due to their rapid response time, high optical contrast, processability and color tunability via structure modifications.[42] In the neutral state, conjugated polymers are insulators. However, by electrochemical or chemical doping/dedoping process, new electronic states, polaron and bipolaron bands, are introduced upon conjugated polymer backbone. With the formation of polaron and bipolaron bands, new charge carriers are obtained and so optical and optoelectronic properties and conductivity of the polymer is improved. Therefore, doping process is one of the main effects for electrochromism of conjugated polymers.[44,45]

The color of the conjugated polymers also depends on the band gap and it can be tuned by doping process. While polymers with band gap greater than 3 eV are colorless in their neutral state, after doping process they absorb light in the visible region. In contrast, polymers with band gap equal or smaller than 1.5 eV absorb light in their neutral state in the visible region, but after doping process they become transparent.[43]

Via structural modification, both band gap and color of the conjugated polymers can also be modulated. For example, alkyl substituted polythiophene is red in its neutral state and green-gray in its oxidized state (**Figure 8**). However, after the addition of electron rich unit to thiophene to form PEDOT, the result is observed in blue color in its neutral state. Due to the increase in HOMO energy level of the conjugated chain and decrease in the band gap by the addition of electron rich unit, absorption of polymer is shifted to red region which is located in longer wavelengths.[45]

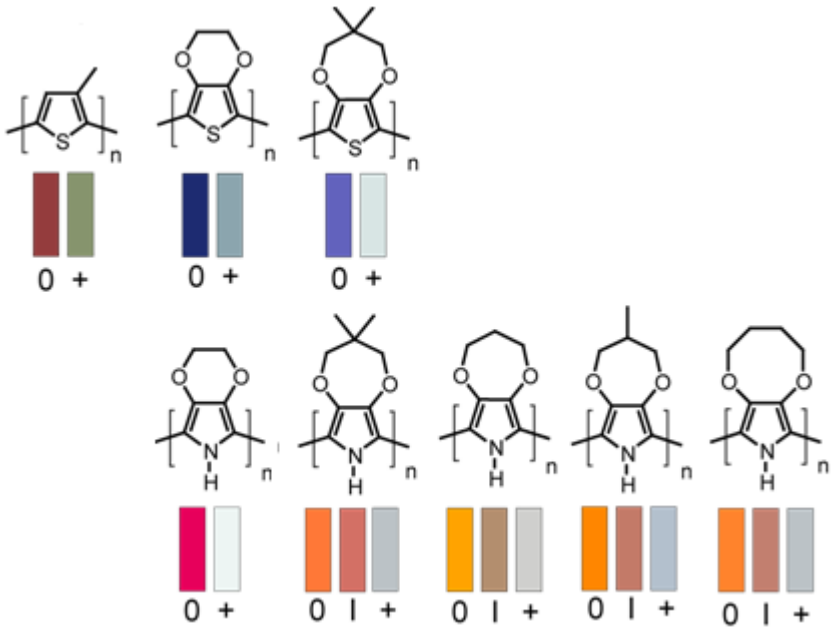

Figure 8. The color change in neutral and oxidized state colors of polythiophene with small alternation in the main polymer backbone[45]

In other words, substitution of electron rich units to the conjugated polymer backbone increases HOMO energy level of the conjugated chain resulting in a narrow band gap. With smaller band gap, optical absorption shifts to longer wavelengths otherwise known as red-shift. On the contrary, addition of electron withdrawing units results in a decrease in LUMO level of the conjugated chain which cause extending band gap. As a results, absorption shifts to shorter wavelengths (blue shift).

1.6. Organic Solar Cells

Sun light is the most important and promising energy source of regenerative energies. By using photovoltaic technology, harvesting energy directly from the sunlight makes inroads into growing global energy consumption. In recent years, organic solar cells which absorbs the light by utilizing π-conjugated polymers in the active layer and converting it into the electricity have drawn attention both in academia and industry. OSCs enable to produce clean, cheap and renewable energy. In contrast to cost-efficiency in large area applications, OSCs provide great potential at a low cost by their simple and cheap fabrication processes. (**Figure 9**) Moreover, the possibility of the modification of moieties on the polymer backbone in combination with the flexible substrates serves a great opportunity in countless ways, from commercial power production to portable technology. However, compared to inorganic solar cells, OSCs have low power conversion efficiencies and they still have a long way to go to compete with inorganic solar cells. Nevertheless, researches are being made to overcome efficiency problem, and they become the focus of extensive studies among the world.[46-50]

Figure 9. Examples of organic solar cell applications[51]

1.6.1. Device Structure of OSCs

1.6.1.1. Single Layer OSC

The single layer organic solar cell device was created by R. N. Marks et al. in 1994 by using poly(p-phenylene vinylene) (PPV) in between ITO anode and Al, Mg, Ca cathodes with a low work function. The quantum efficiency for this device was found as 0.1% under 0.1 mW/cm^2 intensity.[46]

This low quantum efficiency was essentially arising from the low mobility of charges over organic semiconductors. In comparison with high carrier mobility of inorganic crystalline silicon (10^3 cm^2/V.s), the carrier mobility of organic semiconductors is around 10^{-3} cm^2/V.s. This enormous difference indicates that photogenerated charges in organic semiconductors require more time to be collected by corresponding electrodes. This low carrier mobility decreases the quantum efficiency and increases the probability of exciton recombination.[47] The problem can be explained by Schottky model which is shown in **Figure 10**. In this model, a Schottky barrier ensues from an organic layer having an electron donor character and an electrode which is energetically close to vacuum level. The only force to dissociate excitons into free charges is electrostatic forces between two

electrodes. However, this force is generally insufficient to split exciton. Hence, electrons and holes combine without reaching the corresponding electrodes and it gives low efficiency to this type of organic solar cell devices.[48,52] In single layer OSC, exciton dissociates only at the interface of semiconducting organic layer and cathode. Later, it was understood that excitons dissociate more efficiently at the interface of donor and acceptor. Consequently, bilayer organic solar cell was developed comprising donor and acceptor layers separately.[47]

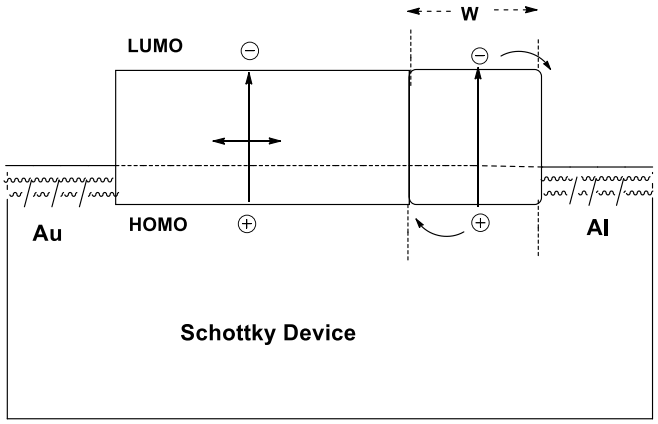

Figure 10. p-type Schottky device

1.6.1.2. Bilayer OSC

The bilayer heterojunction device structure (**Figure 11**) containing a p-type layer for hole transport and a n-type layer for electron transport was found by C. W. Tang in 1985 in order to improve solar cell quantum efficiency.[50-53] The device structure was indium tin oxide (ITO)/copper phthalocyanine (CuPc) / perylene tetracarboxylic derivative (PV) / silver (Ag). The quantum efficiency for this device was found as 1% under AM 2 conditions. This increase in power conversion efficiency (PCE) is arising from increasing exciton dissociation possibility by adding electron transport layer which forms an energy offset at the hole transport layer interface.[48,54-56]

However, due to excitons' short life time (typically in the range of 100 ps to 1 ns), donor-acceptor layers' thickness is limited by the exciton diffusion length which is less than optical absorption depth. Organic materials have usually 10-20 nm exciton diffusion length and 100nm optical absorption depth.[48] In such devices, excitons occur at the small area of donor-acceptor interface and if the donor or acceptor layer is too thick, generated excitons far from the heterojunction may recombine without having a chance to reach the acceptor.[52] Moreover, thicker layers result minimum photocurrent at the maximum of the optical absorption spectrum due to optical filter effect of the absorbing material.[49] All those reasons lead to loss of excitons, absorbed photons and quantum efficiency. To overcome these tradeoff factors, a new heterojunction was found: Bulk Heterojunction (BHJ).[52]

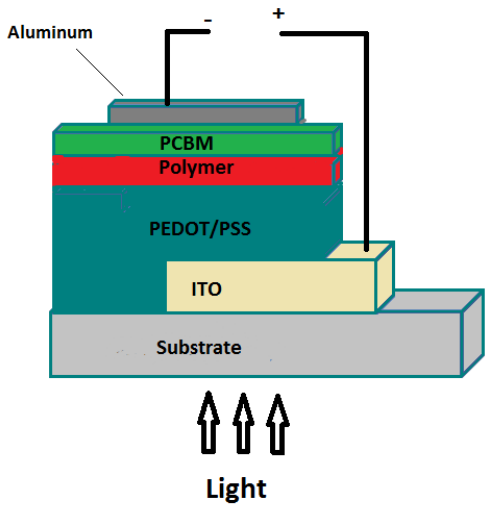

Figure 11. Bilayer heterojunction device structure

1.6.1.3. Bulk Heterojunction OSC

Bulk heterojunction is a blend of donor and acceptor moieties which exhibits a donor-acceptor phase separation in a 10-20 nm length scale.[49] It serves much larger interface between donor and acceptor for exciton dissociation in the active layer and thus reduces

the distance exciton needs to travel to reach interface and resulted in improved quantum efficiency for organic solar cells.[48,49] The breakthrough development of BHJ solar cells was reported by Heeger and co-workers from the discovery of efficient charge transfer in conjugated polymer- fullerene blend.[52]

In this system (**Figure 12**), active layer containing conjugated polymer as donor and fullerene derivatives as acceptor is sandwiched between two electrodes.[48] Buckminster-fullerene (C_{60}) is known as an ideal n-type material due to its relatively low lying LUMO energy level which provides thermodynamically favorable energy state for accepting electrons from an excited p-typed material (conjugated polymer). Fullerene derivatives have high mobility but also poor solubility. To overcome this problem for the first time, by Wudl and Hummelen in 1995, soluble [6,6]-phenyl-C_{61} –butyric acid methyl ester ($PC_{61}BM$) was synthesized and used for BHJ solar cells. The efficiency of BHJ solar cell can be improved by replacing $PC_{61}BM$ with $PC_{71}BM$ which has lower symmetry and absorbs more light in visible region.[52]

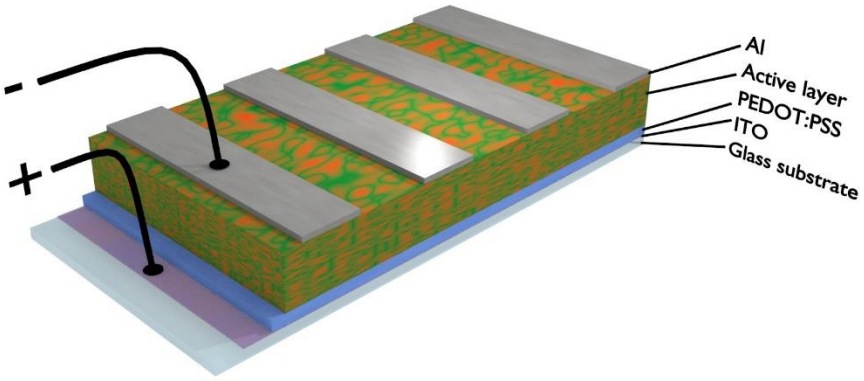

Figure 12. Bulk heterojunction device structure

In contrast to bilayer heterojunction which has donor and acceptor materials separately, in the bulk heterojunction an interpenetrating area of donor acceptor is involved in the active layer. This single layer simplifies the fabrication of the device by using solution processing methods without struggling on interfacial erosion problems mostly happening in bilayer configuration.[52] There is no exact symmetry or no net direction where exciton should travel in the bulk heterojunction. Thus, symmetry disorder is critical in BHJ. Free electrons and holes require percolated pathways for free charge transporting phases to the electrodes. In other words, the donor-acceptor phases should form bicontinuous, nanoscale, and interpenetrating pathways. Therefore, morphology is more essential in BHJ devices.[49]

1.6.2. Working Principle of OSCs

In the organic cell working principle, there are six major steps to convert the light to electricity as shown in the **Figure 13**[57]**.** Process begins with the photon absorption by the conjugated polymers in the active layer which leads to exciton formation. After exciton formation, bound electron-hole pairs diffuse within the organic semiconductor independent on the applied electric field. Additionally, an acceptor molecule as fullerene derivatives are needed to produce a junction area to bring in electrostatic forces at the interface. Exciton diffusion length is mostly 10-20 nm and exciton dissociates only at the donor-acceptor interface due to the offset of LUMO levels of donor and acceptor materials. If excitons do not reach the interface, they fall back to the ground state and recombine. Therefore, to generate efficient power, excitons have to be dissociated and collected by corresponding electrodes before recombination.[58-61]

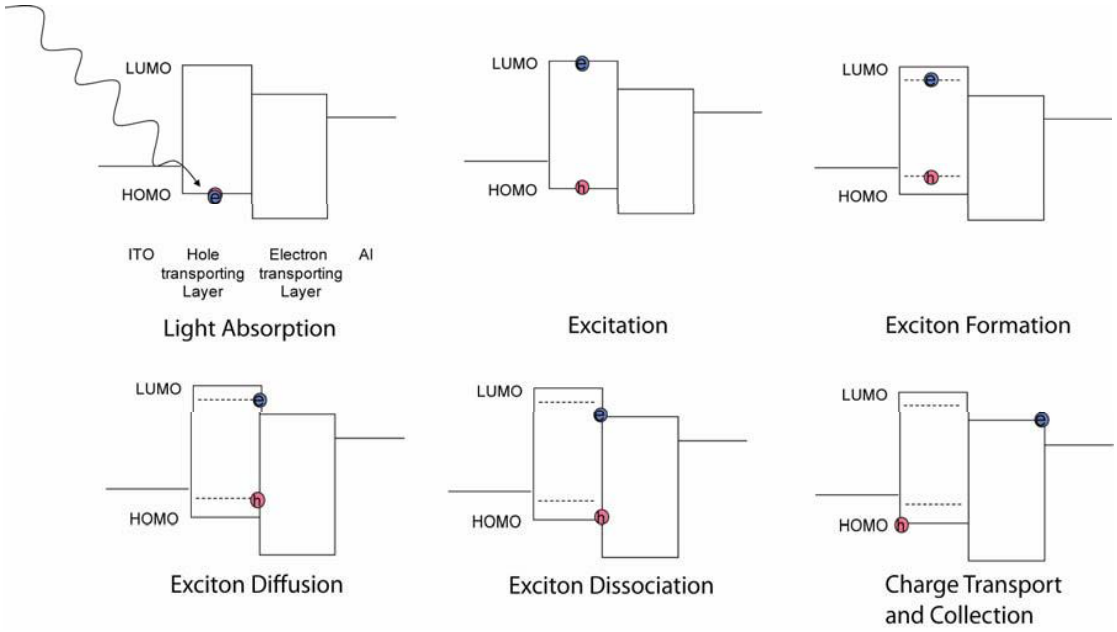

Figure 13. Working principle of OSC[57]

1.6.3. Characterization of an Organic Solar Cell Device

The efficiency and characteristics of an organic solar cell can be defined by the current density-voltage (J-V) graph which is shown in the **Figure 14.** According to this graph, there are two different conditions for the cell; under dark and illumination. In the dark, the JV curve passes through the origin with almost no current flow or potential. Yet, when the device is under the light, in the fourth quadrant it shows current flow and potential, in other words, it generates power. The power conversion efficiency of an organic solar cell is calculated by the equations below:

$$\eta_e = \frac{P_{max}}{P_{in}} \qquad FF = \frac{J_{max} * V_{max}}{I_{sc} * V_{oc}} \qquad P_{max} = V_{oc} * J_{sc} * FF$$

Where η_e is the power conversion efficiency (PCE) value, J_{sc} is short circuit current, V_{oc} is open circuit voltage, P_{in} is the incident light and FF is the fill factor. AM 1.5 G (Air Mass 1.5 Global) is taken as a standard source in all the measurements.[58] Air mass is a measurement to calculate how much sunlight travels through the atmosphere to reach the surface of the earth. During this passage, sunlight might be reduced by absorption and reflection due to the dusts, water vapor and clouds or by scattering. The international AM is taken as AM 1.5 for solar cells which means sunlight reaches to the earth surface with the angle of 48 ^{o}. It's not the light intensity, it's the spectrum of radiation. Therefore the intensity is fixed at 100 mW/cm^2 for solar cell measurements.[47-49]

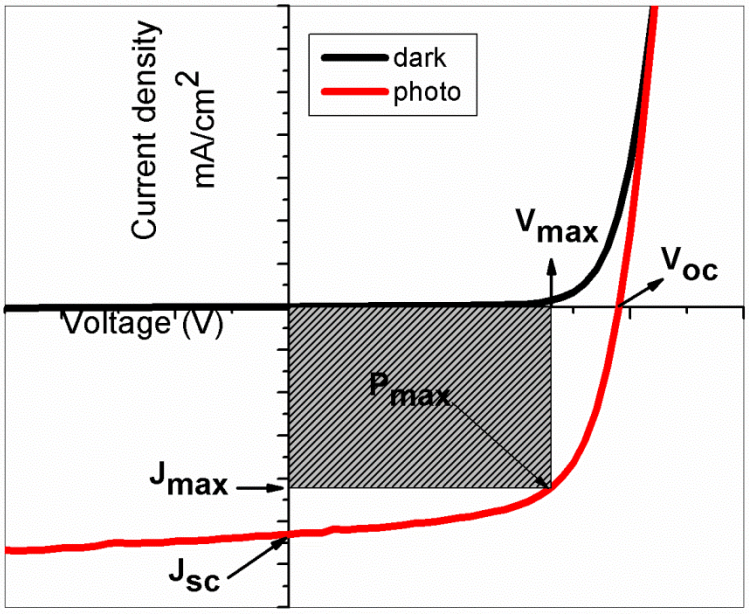

Figure 14. Current density voltage graph

1.6.4. Critical Parameters Affecting OSC Efficiency

1.6.4.1.Open-Circuit Voltage (V_{oc})

The open circuit voltage is measured by the difference in work functions of two metal contacts in metal-insulator-metal (MIM) devices. However, in p-n junctions, it is calculated by the difference of the quasi Fermi levels of n-doped and p-doped semiconductor energy levels[49]. V_{oc} is defined as the maximum potential voltage across the organic solar cell when there is no current flowing.[47] In organic solar cells, V_{oc} is linearly depends on the HOMO level of p-type semiconductor quasi Fermi level (donor) and LUMO level of the n-type semiconductor quasi Fermi level (acceptor). This linear correlation was found by Brabec et al in 2001 by using first reduction potential (LUMO) of the fullerene acceptors. Later on, in 2006, Scharber et al studied numerous different bulk heterojunction solar cells and showed the linear relation between V_{oc} and oxidation potential of the conjugated polymers. As a result of these studies, the following equation was obtained to calculate V_{oc}. Deviations between the theoretical maximum built-in potential (V_{BI}) and V_{oc} on the order of 0.3 V are found.[62,63]

$$\mathbf{V_{oc} = (1/q)\,[E\,(HOMO)_{donor} - E\,(LUMO)_{acceptor}] - 0.3\ V}$$

1.6.4.2.Short-Circuit Current (J_{sc})

Short circuit current (J_{sc}) is the the maximum current across the solar cell when there is no externally applied voltage or simply when the device is short circuited.[47] J_{sc} depends on the number of charge carriers generated and collected at the corresponding electrodes at the short circuited. By the help of smaller band gap or phase separation, and higher absorption coefficient or carrier mobility can increase J_{sc} value.[52]

The J_{sc} is directly related with external quantum efficiency (EQE) which is the ratio between the number of all the incident photons on the solar cell device and the number of collected charge carriers at a given wavelength.[64,65]

$$(EQE = \eta_{abs*}\ \eta_{diff*}\ \eta_{diss*}\ \eta_{tr*}\ \eta_{cc})$$

EQE can be calculated by the following formula where the η_{abs} is a parameter which is related to the light absorption efficiency.[66,67] η_{diff} is the capability parameter which is related to the diffusion of the electron-hole pairs to the donor-acceptor interface.[68,69] η_{diss} is explained by dissociation efficiency of excitons where η_{tr} is the charge transfer efficiency.[65,69,70] Lastly, η_{cc} is the efficiency parameter based on the ability of electrodes to charge collection.[65]

EQE is also referred as incident photon to current efficiency (IPCE) which is the ratio of the number of collected photons under the short circuit to the number of incident photons through solar cell.[47,49] IPCE is calculated by following equation where J_{sc} is the photo current of the device, P_{in} is the incident power, and λ is the incident photon wavelength.[47]

$$IPCE = 1240J_{sc} / \lambda P_{in}$$

1.6.4.3.Fill Factor (FF)

Fill factor (FF) is the mainspring to determine the power conversion efficiency for organic solar cells. FF which is defined as the ratio of the maximum power (P_{max}) to product of V_{oc} and J_{sc} depends on the relation between recombination and transportation of charge carriers. Increase in the recombination ratio affects FF inversely. As shown in the **Figure 14** as the square edge of the graph increases, FF correlatively increases. However, FF is also related to diode quality which may lead to deviate from the theoretical ideal value of J-V curve. This aberration can be explained by the fluctuations on the two main parameters: Series resistance (R_s) and shunt resistance (R_{sh}). For an ideal diode, R_s should be zero while R_{sh} goes to infinity. R_{sh} is simply the parameter of recombination of charge carriers near the D-A interface. This can be estimated by taking the inverse slope around 0 V. Decrease in R_{sh} leads to alternative current paths which reduce the current flow though the organic solar cell. In other respects R_s is responsible from the charge carrier mobility. R_s increases in the presence of traps which diminish the number of charge

carriers leading to increase in the travelling distance of carriers. This can be derivated from the slope at a positive voltage V_{oc} where the J-V curve becomes linear.[65,71]

1.7. Benzotriazole and Quinoxaline Containing Polymer Solar Cells

Benzotriazole (BTz) containing polymers revealed superior properties in electrochromic and photovoltaic cell applications. Most of the BTz derivatives showed multicolored character and highly transmissive states which are very essential parameter for electrochromic devices.[72] Due to the diamine structure BTz is used the moderately electron-deficient unit in D-A type conjugated polymers.[73] Low electron accepting property of BTz leads to high LUMO energy level and high band gap consequently.[72] Therefore, BTz is not chosen as often as quinoxaline and benzothidiazole strong acceptor units for polymer solar cell structures.[74] However, it can be easily modified with alkyl groups at one of the nitrogen atoms on the triazole unit to achieve higher solubility which resulted 7% power conversion efficiency in polymer solar cells.[75] Hence, different moieties were selected to combine with BTz to improve electrochemical and photovoltaic cell properties of conjugated polymers in terms of optical contrast, switching times, processability, lower band gap and high power conversion efficiency.[72]

Among the D-A approach to obtain low band gap conjugated polymers quinoxaline derivates have been widely used as acceptor units owing to electron withdrawing property of two imine nitrogens on the structure. Quinoxaline unit has a fascinating structure for modification and control over electrochemical and photovoltaic cell properties. Different substituents can be tailored easily to quinoxaline structure from 2 and 3 positions.[29] In 2010, E. Wand and coworkers reported that 5,8-dithien-2-yl-2,3-diphenylquinoxaline structure polymerized with thiophene showed up to 6% PCE with a blend of **TQ1:$PC_{61}BM$** (weight ratio is 1:3).[76] However, the same quinoxaline structure polymerized with carbazole or fluorine units by M. H. Lai group in 2009 and Y. L. Yang group in 2010 and polymer revealed poorer photovoltaic performance with PCEs less than 2%.[77,78] Later on, instead of phenyl rings, in 2011, Jen group reported

PIDTphanQ:PC$_{71}$BM (weight ratio is 1:3) quinoxaline derivate containing fused-phenyl rings was achieved 6.24% PCE of OSCs[79] (**Figure 15**). It was proven that fused-phenyl rings reduce the energetic disorder of the polymer backbone after facilitating polymer coplanarity and interchain π-π interactions which enable higher FF and PCE in OSCs.[28]

a)

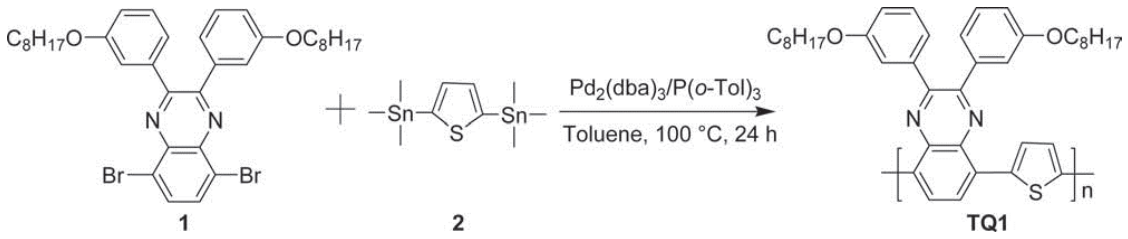

b)

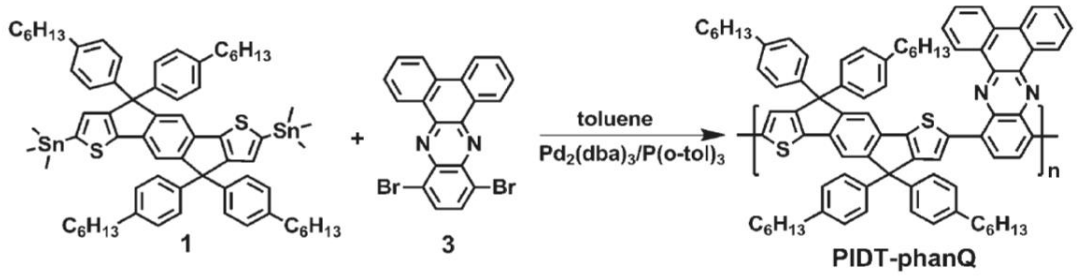

Figure 15. Synthesis of **TQ1** (6% PCE) (a) and **PIDT-phanQ** (6.24% PCE) (b)

1.8. Aim of the Study

Donor-acceptor approach is the most commonly used method to achieve low band gap polymers resulting high power conversion efficiency for organic solar cell devices. In the fabrication of organic solar cells, bulk heterojunction is the most efficient system to achieve higher power conversion efficiency owing to the significantly extended donor-

acceptor interface. For that purpose, donor-acceptor type random copolymers via altering acceptor units on the polymer backbone were synthesized to achieve broad light absorption in visible spectrum for bulk heterojunction polymer solar cell applications. Three novel polymers, **CoP1, CoP2** and **CoP3**, containing 5,8-dibromo-2,3-di(thiophen-2-yl)quinoxaline, 5,8-dibromo-2,3-diphenylquinoxaline, 10,13-dibromodibenzo[a,c]phenazine acceptor units combined with 4,7-dibromo-2-(2-octyldodecyl)-2H-benzo[d][1,2,3]triazole were synthesized via Stille coupling. Then, optoelectronic properties and organic solar cell applications of the copolymers were completed. Structures of copolymers were indicated below in **Figure 16**.

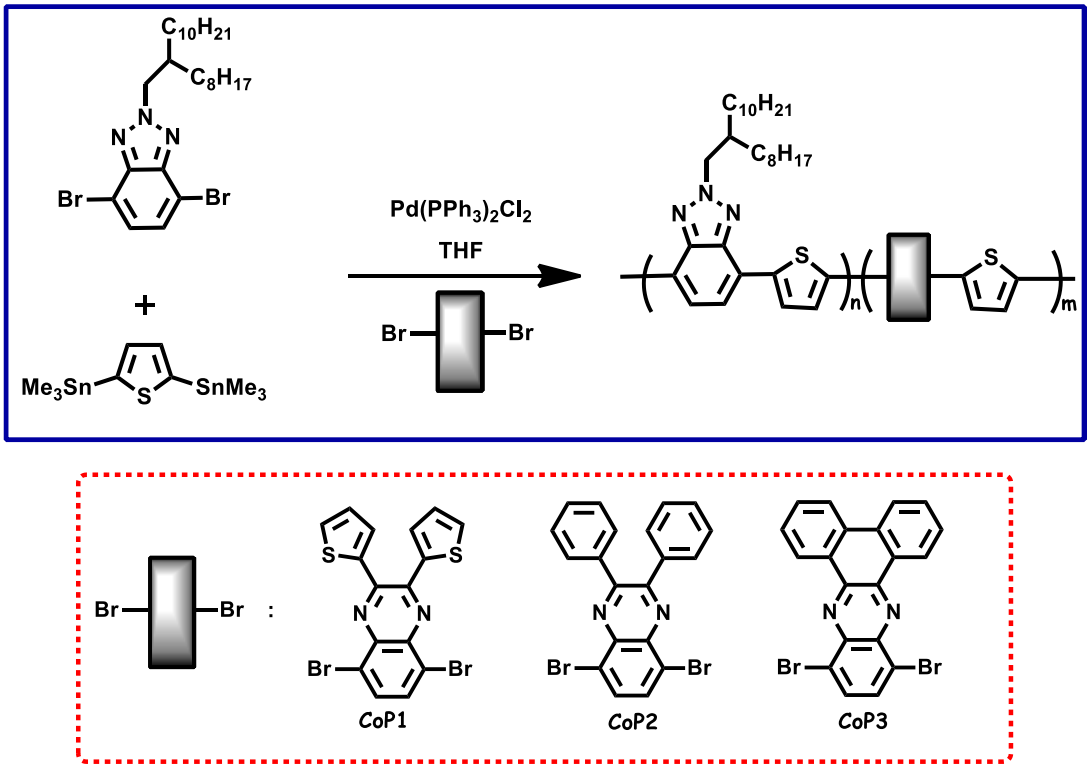

Figure 16. Synthesized copolymers **CoP1, CoP2** and **CoP3**

CHAPTER 2

2. EXPERIMENTAL

2.1. Materials and Equipments

All chemicals used in the synthesis of monomers and polymers were purchased from Sigma-Aldrich Chemical Co. Ltd. The $PC_{71}BM$ which was used in the device fabrication was purchased from Solenne. Tetrahydrofuran (THF) and toluene were dried by using metallic sodium and benzophenone and freshly used in the reactions. Other solvents were used as received without any further drying operation. Reactions especially moisture and air sensitive ones were performed under argon atmosphere unless otherwise mentioned.

For the purification of the materials, Merck Silica Gel 60 was used as the stationary phase with different corresponding mobile phase solvents in the column chromatography. Chemical structures of the monomers and polymers were proven by ^{1}H and ^{13}C NMR spectra in $CDCl_3$. They were recorded on a Bruker Spectrospin Avance DPX-400 Spectrometer with respect to trimethylsilane (TMS) the internal reference. In the $CDCl_3$ solvent, according to the TMS reference, the chemical shifts were stated at 7.26 ppm for ^{1}H and 77 ppm for ^{13}C NMR. Average molecular weights of the polymers were calculated by gel permeation chromatography (GPC) with polystyrene standard in chloroform ($CHCl_3$). Thermal analysis of the polymers were studied by thermogravimetry analysis (TGA) and differential scanning calorimetry (DSC). Perkin Elmer Pyris 1 TGA was used under nitrogen (N_2) atmosphere with a 10 ^{o}C/min heating rate up to 950 ^{o}C and decomposition temperature (T_d) was found. In order to clarify melting point (T_m) and glass

transition temperature (T_g), Perkin Elmer DSC Diamond was used under N_2 atmosphere with a 10 ^oC/min heating rate up to 300 ^oC.

2.2. Synthesis of Monomers

2.2.1. Synthesis of 9-(bromomethyl)nonadecane (1)

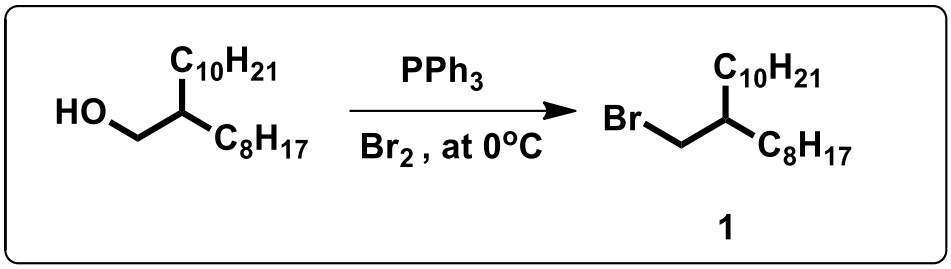

Figure 17. Synthesis of 9-(bromomethyl)nonadecane

2-Octyl-1-dodecanol (10 g, 33.5 mmol) and triphenylphosphine PPh_3 (9.22 g, 35.15 mmol) were dissolved in 75 mL dichloromethane (DCM) and reaction mixture was cooled down to 0^oC. Bromine (1.8 mL, 35 mmol) was added to reaction mixture and mixture was stirred for 30 minutes at 0^oC. Then, reaction was warmed to room temperature and stirred for additional 30 minutes. $NaHSO_3$ solution was added to the reaction mixture to get rid of excess Br_2. By the addition of $NaHSO_3$ solution, dark yellow solution turns into faint yellow in a while. Organic phase was washed with DCM, water and brine. After the extraction, organic phase was dried over $MgSO_4$ and evaporated to obtain white solid. Purification of crude product was performed with column chromatography on silica gel by using hexane and 9-(bromomethyl)nonadecane was obtained as colorless oil (12 g, 94%) ^1H NMR (400 MHz, $CDCl_3$), δ (ppm): 3.37(d, *J*=4.7 Hz, 2H), 1.52 (m,1.46-1.57, 1H), 1.20 (m,1.15-1.32, 32 H), 0.81 (t, *J*=6.58 Hz , 6H).^{13}C NMR (100 MHz, $CDCl_3$), δ (ppm): 39.6, 39.5, 32.59, 31.9, 29.8, 29.7, 29.6, 29.5, 29.4, 29.3, 26.6, 22.7, 14.1.

2.2.2. Synthesis of 4,7-dibromobenzo[c][1,2,5]thiadiazole (2)

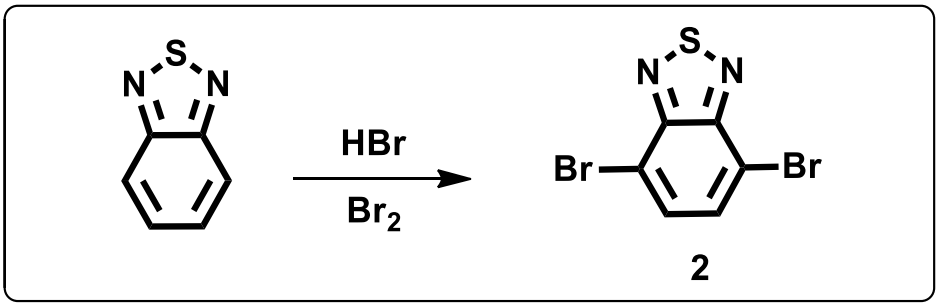

Figure 18. Synthesis of 4,7-dibromobenzo[c][1,2,5]thiadiazole

Benzo-1,2,5-thiadiazole (5.0 g, 36.7 mmol) was dissolved in 40 mL HBr (47%) in room temperature. Later, a solution of Br_2 (17.6 g, 110 mmol) in 30 ml HBr was added dropwise to reaction mixture. After the addition of Br_2, the reaction mixture was heated to 135 ^oC and refluxed for overnight. Then the mixture was cooled down to room temperature and $NaHSO_3$ solution was added to get rid of excess Br_2.. The mixture was filtered and orange solid was washed with cold diethyl ether and water several times to obtain 4,7-dibromobenzo[c][1,2,5]thiadiazole (9.53 g, yield 88%) as a yellow solid. ^1H NMR (400 MHz, $CDCl_3$) δ (ppm): 7.66 (s, 2H). ^{13}C NMR (100 MHz, $CDCl_3$) δ (ppm): 152.9, 132.3, 113.9.

2.2.3. Synthesis of 3,6-dibromobenzene-1,2-diamine (3)

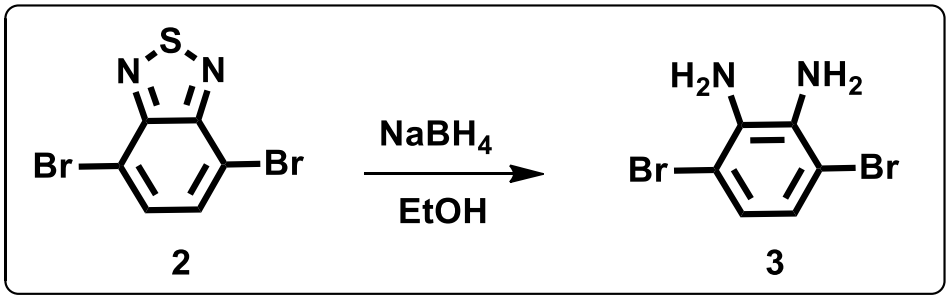

Figure 19. Synthesis of 3,6-dibromobenzene-1,2-diamine

4,7-Dibromobenzothiadiazole (5.0 g, 17 mmol) was dissolved in 50 mL ethanol (EtOH) in 1L-rounded flask. The reaction mixture was cooled down to 0^{o}C and $NaBH_4$ (1.7 g, 0.51 mol) was added to reaction mixture in portions. The reaction was stirred in the ice bath until gas evolution was stopped and then stirred for 20 hours in room temperature. After the evaporation of ethanol, extraction was performed with water and diethyl ether. Extraction was carried out once again with brine to obtain faint yellow organic phase. Later, the organic phase was dried over $MgSO_4$, evaporated under reduced pressure and a faint yellow solid, 3,6-dibromobenzene-1,2-diamine(3.5 g, yield 80%) was obtained. The product is time-sensitive, in couple of days, it may disintegrate. ^{1}H NMR (400 MHz, $CDCl_3$) δ (ppm): 6.78 (s, 2H), 3.82 (s, 4H). ^{13}C NMR (100 MHz, CDCl3) δ (ppm): 133.5, 123.2, 109.5.

2.2.4. Synthesis of 4,7-dibromo-2H-benzo[d][1,2,3]triazole (4)

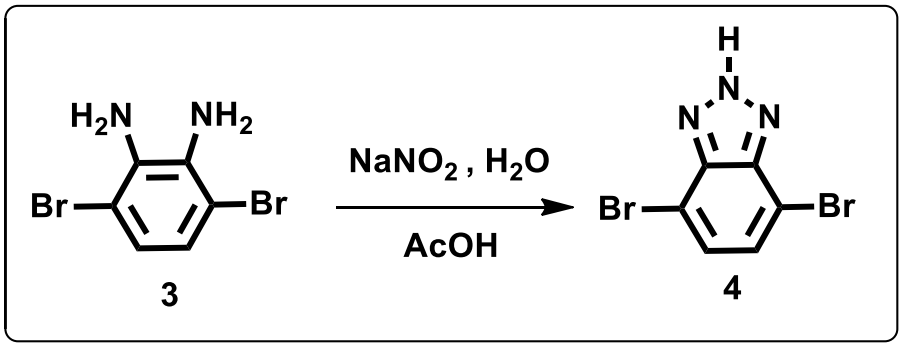

Figure 20. Synthesis of 4,7-dibromo-2H-benzo[d][1,2,3]triazole

To a solution of 3,6-dibromobenzene-1,2-diamine (0.8 g, 3 mmol) in 12 mL acetic acid (AcOH), a solution of $NaNO_2$ (0.3g, 3.3 mmol) in 6 mL H_2O was added drop wise at room temperature. After 30 minutes stirring, the powder was filtered and washed with distilled water several times to afford 4,7-dibromo-2H-benzo[d][1,2,3]triazole as a pink powder (80% yield).

2.2.5. Synthesis of 4,7-dibromo-2-(2-octyldodecyl)-2H-benzo[d][1,2,3]triazole (5)

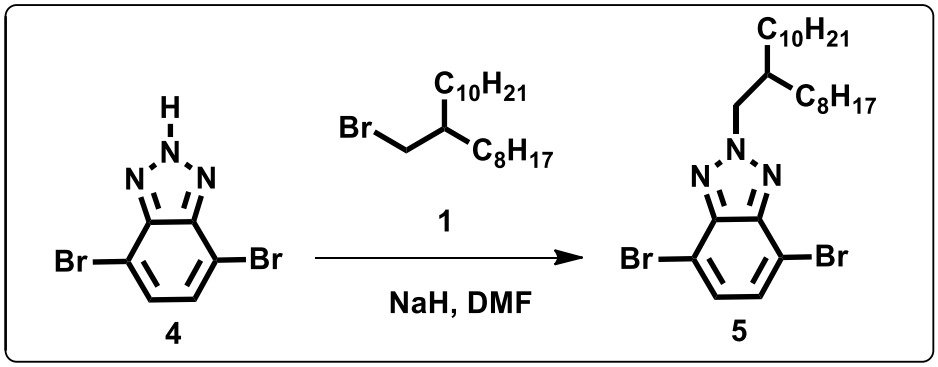

Figure 21. Synthesis of 4,7-dibromo-2-(2-octyldodecyl)-2H-benzo[d][1,2,3]triazole

4,7-Dibromo-2H-benzo[d][1,2,3]triazole (3.0 g, 7.22 mmol) was dissolved in 10 mL dimethylformamide (DMF) under argon atmosphere and reaction medium was cooled down to 0^{o}C. Then, NaH (312 mg, 8.75 mmol) was added to reaction mixture at 0 ^{o}C. After completion of addition, the reaction was heated to 60 ^{o}C. 9-(bromomethyl)nonadecane (4.68 g, 12.96 mmol) was added to reaction medium. The reaction was stirred at 65-70 ^{o}C overnight. The reaction mixture was extracted with chloroform ($CHCl_3$) and water. The organic phase was extracted with brine and chloroform once again. The organic residue was dried over $MgSO_4$ and evaporated. Column chromatography on silica gel with hexane and $CHCl_3$ (1:3) yielded 4,7-dibromo-2-(2-octyldodecyl)-2H-benzo[d][1,2,3]triazole as a faint yellow oil (2.3 g, yield 40%). ^{1}H NMR (400 MHz, $CDCl_3$), δ (ppm): 7.32 (s, 2H), 4.59 (d, = 7.3 Hz, 2H), 2.25 (m, 2.19–2.30, 1H), 1.13 (m, 1.08–1.30, 32H), 0.78 (m, 0.75–0.80, 6H). ^{13}C NMR (100 MHz, $CDCl_3$), δ (ppm): 141.4, 127.2, 107.8, 58.9, 36.8, 29.7, 29.6, 29.4, 29.0, 27.6, 27.4, 27.3, 27.2, 27.1, 27.0, 23.8, 20.5, 20.4, 11.9.

2.2.6. Synthesis of 2,5-bis(trimethylstannyl)thiophene (6)

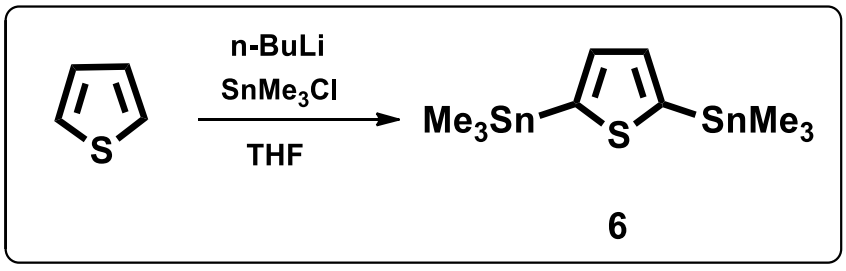

Figure 22. Synthesis of 2,5-bis(trimethylstannyl)thiophene

2,5-Dibromothiophene (1.5 g, 6.2 mmol) was dissolved into 40 mL dry THF at -78^{o}C under argon atmosphere. 2.5 M n-butyllithium (n-BuLi) solution (5.95 mL, 14.88 mmol) was added drop wise into the solution mixture and stirred for 1 hour under the same

conditions. Later, 1 M trimethyltin chloride ($SnMe_3Cl$) (15.5 mL, 15.5 mmol) was added and stirred for 5 minutes at -78 ^oC. Solution mixture was stirred overnight at room temperature under argon atmosphere. After the evaporation of the solvent, the resulting mixture was extracted with diethylether and water several times. The organic phase was dried with $MgSO_4$ and evaporated under vacuum. The yellowish solid was washed with cold methanol a few times to obtain white crystal solid. (1 g; yield = 39.2 %) ^1H NMR ($CDCl_3$, 400 MHz): δ (ppm) 7.46 (s, 2H), 0.34 - 0.52 (m, 18H).

2.2.7. Synthesis of quinoxaline derivatives

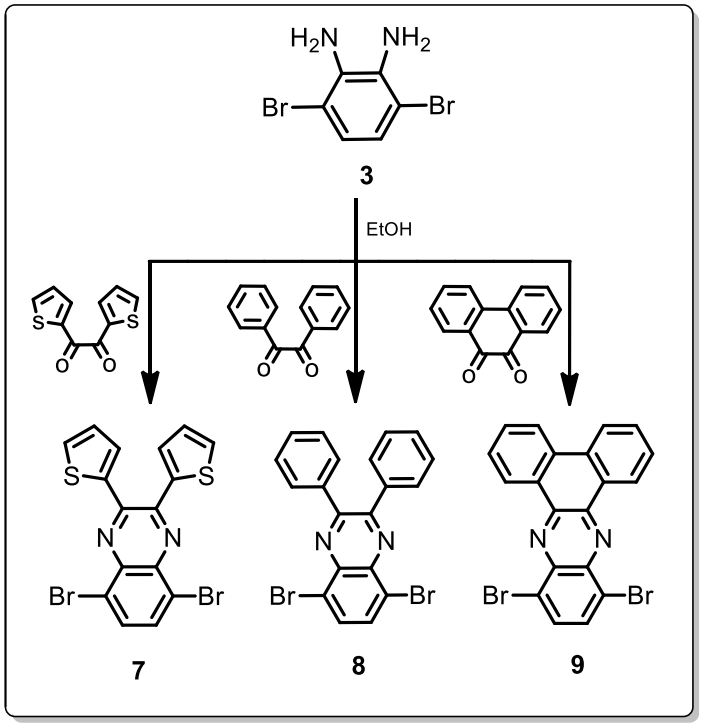

Figure 23. General synthetic pathway for all additional acceptor units (7-8-9)

2.2.7.1 Synthesis of 5,8-dibromo-2,3-di(thiophen-2-yl)quinoxaline (7)

3,6-Dibromobenzene-1,2-diamine (3) (200 mg, 0.752 mmol) and 1,2-di(thiophen-2-yl)ethane-1,2-dione (418 mg, 1.88 mmol) were dissolved in the 25 mL ethanol at room temperature. The solution mixture was heated for few minutes and later on catalytic amount of PTSA was added. The desired solid was precipitated with PTSA addition. The mixture was refluxed at 100^{o}C overnight. The precipitate was filtered and washed with ethanol to obtain yellow solid. (88% yield) ^{1}H (400 MHz, $CDCl_3$) δ (ppm): 7.77 (s, 2H), 7.49 (dd, 2H), 7.41 (dd, 2H), 6.98 (s, 2H).

2.2.8. Synthesis of 5,8-dibromo-2,3-diphenylquinoxaline (8)

3,6-Dibromobenzene-1,2-diamine (3) (200 mg, 0.752 mmol) and benzil (395 mg, 1.88 mmol) were dissolved in the 25 mL ethanol at room temperature. The solution mixture was heated for few minutes and later on catalytic amount of PTSA was added. The desired solid was precipitated with the PTSA addition. The mixture was refluxed at 100^{o}C overnight. The precipitate was filtered and washed with ethanol to obtain yellow solid (94% yield). ^{1}H (400 MHz, $CDCl_3$) δ (ppm): 7.84 (s, 2H), 7.56 (dd, 2H), 7.48 (dd, 2H), 7.05 (s, 2H).

2.2.9. Synthesis of 10,13-dibromodibenzo[a,c]phenazine (9)

3,6-Dibromobenzene-1,2-diamine (3) (200 mg, 0.752 mmol) and phenanthrene-9,10-dione (391 mg, 1.88 mmol) were dissolved in the 25 mL ethanol at room temperature. The solution mixture was heated for few minutes and later on catalytic amount of PTSA was added. The desired solid was precipitated with the PTSA addition. The mixture was refluxed at 100^{o}C overnight. The precipitate was filtered and washed with ethanol to obtain yellow solid 88% yield). ^{1}H (400 MHz, $CDCl_3$) δ (ppm): 9.41 (d, *J*=1.5 Hz, 2H), 8.50 (dd, *J*=1.5, 2H), 7.96 (s, 2H), 7.75 (t, 4H).

2.3. Synthesis of Polymers

2.3.1. Synthesis of CoP1

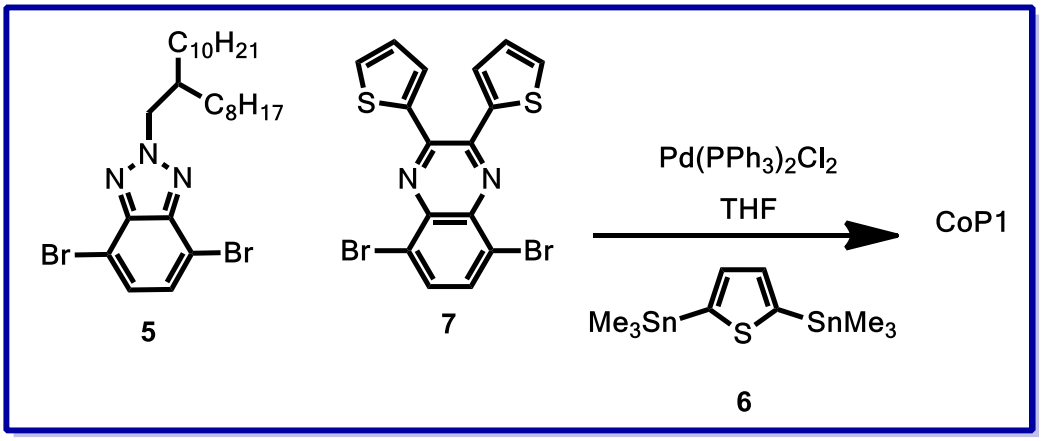

Figure 24. Synthetic route for copolymer **CoP1**

CoP1 was synthesized via Stille coupling reaction by mixing 4,7-dibromo-2-(2-octyldodecyl)-2H-benzo[d][1,2,3]triazole (5) (0.247 g, 0.442 mmol) and 5,8-dibromo-2,3-di(thiophen-2-yl)quinoxaline (7) (0.200 g, 0.442 mmol) and 2,5-bis(trimethylstannyl)thiophene (6) (0.362 g, 0.883 mmol) in 8mL dry THF in room temperature under argon atmosphere. The solution mixture was bubbled with argon for a while in order to remove air. After bubbling, catalyst tris(dibenzylideneacetone)dipalladium(0) (5.0 mol %, 0.02 g) and co-catalyst tris(o-tolyl)phosphine (11.0 mol %, 0.015 g) were added into solution mixture and refluxed at 70^{o}C for 36 hours under argon atmosphere. 2-Bromothiophene (0.216 g, 1.327 mmol) and catalytic amount of extra catalyst were added and the solution mixture was stirred for 6 hours. Later on, trimethyl(thiophen-2-yl)stannane (0.99 g, 2.654 mmol) and catalytic amount of extra catalyst were added and stirred for 6 hours under same conditions. The reaction was cooled to room temperature and precipitated in cold methanol. Filtered

mixture was purified by Soxhlett apparatus. Purification was made firstly with acetone and then with hexane to remove oligomers, small molecules and excess catalyst and co-catalyst. The polymer **CoP1** was collected by chloroform and then the solvent was evaporated under vacuum. The solid residue was precipitated in cold methanol. Pure polymer was collected by vacuum filtration.

GPC: Mn: 246.8 kDa, Mw: 589 kDa, PDI: 2.38.

^{1}H NMR (400MHz, $CDCl_3$) δ (ppm): 7.9 (benzotriazole), 7.7 (quinoxaline), 7.3 (thiophene), 7.0 (benzene), 4.7 (N-CH_2), 2.2 (C-CH_2), 1.9-0.5 (pendant alkyl chains).

2.3.2. Synthesis of CoP2

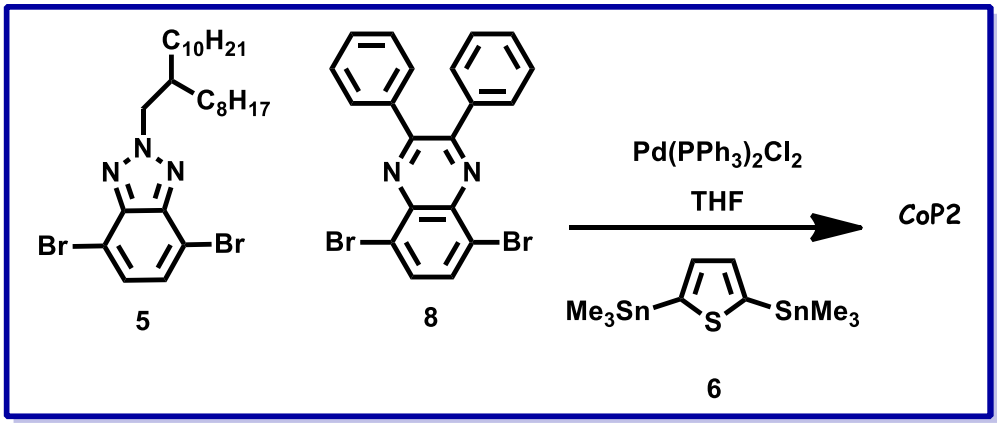

Figure 25. Synthetic route for copolymer **CoP2**

The same procedure with the synthesis of **CoP1** was followed to synthesize **CoP2**. In this manner, 4,7-dibromo-2-(2-octyldodecyl)-2H-benzo[d][1,2,3]triazole (5) (0.388 g, 0.696 mmol) and 5,8-dibromo-2,3-diphenylquinoxaline (8) (0.306 g, 0.696 mmol) and 2,5-bis(trimethylstannyl)thiophene (6) (0.571 g, 1.392 mmol) in 8mL THF in room temperature under argon atmosphere. The solution mixture was bubbled with argon for a while in order to remove air. After bubbling, catalyst tris(dibenzylideneacetone)dipalladium(0) (5.0 mol %, 0.032 g) and co-catalyst tris(o-

tolyl)phosphine (11.0 mol %, 0.023 g) were added into solution mixture and refluxed at 70^{o}C for 36 hours under argon atmosphere. 2-Bromothiophene (0.340 g, 2.088 mmol) and catalytic amount of extra catalyst were added and the solution mixture was stirred for 6 hours. Later on, trimethyl(thiophen-2-yl)stannane (1.56 g, 2.654 mmol) and catalytic amount of extra catalyst were added and stirred for 6 hours under same conditions. The reaction was cooled to room temperature and precipitated in cold methanol. Filtered mixture was purified by Soxhlett apparatus. The polymer **CoP2** was collected by chloroform and then the solvent was evaporated under vacuum. The solid residue was precipitated in cold methanol. Pure polymer was collected by vacuum filtration.

GPC: Mn: 69.2 kDa, Mw: 256 kDa, PDI: 3.7.

^{1}H NMR (400MHz, $CDCl_3$) δ (ppm): 7.9 (benzotriazole), 7.7 (quinoxaline), 7.3 (thiophene), 7.0 (benzene), 4.7 (N-CH_2), 2.2 (C-CH_2), 1.9-0.5 (pendant alkyl chains).

2.3.3. Synthesis of CoP3

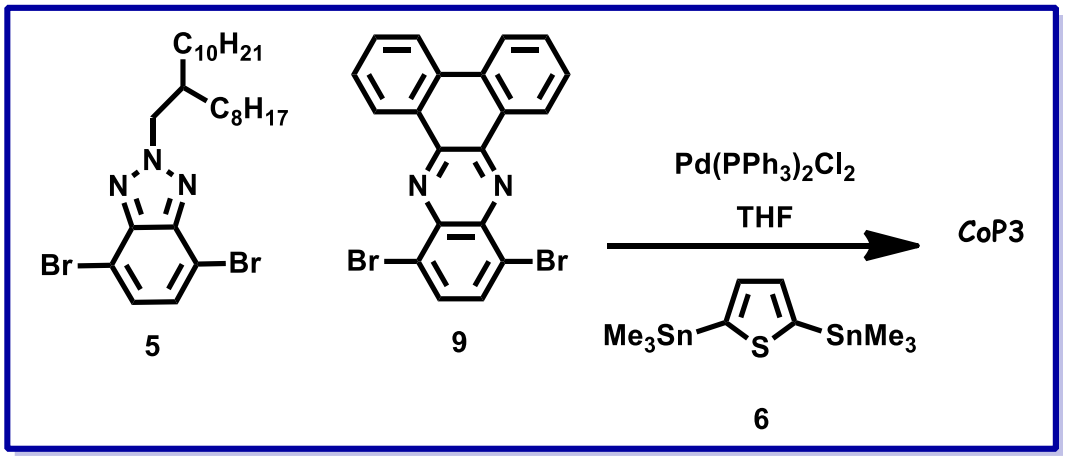

Figure 26. Synthetic route for copolymer **CoP3**

The same procedure with the synthesis of **CoP1** was followed to synthesize **CoP3**. In this manner, 4,7-dibromo-2-(2-octyldodecyl)-2H-benzo[d][1,2,3]triazole (5) (0.254 g, 0.456

mmol) and 10,13-dibromodibenzo[a,c]phenazine (9) (0.200 g, 0.456 mmol) and 2,5-bis(trimethylstannyl)thiophene (6) (0.374 g, 0.912 mmol) were mixed in 8mL THF at room temperature under argon atmosphere. The solution mixture was bubbled with argon for a while in order to remove air. After bubbling, catalyst tris(dibenzylideneacetone)dipalladium (0) (5.0 mol %, 0.021 g) and co-catalyst tris(o-tolyl)phosphine (11.0 mol %, 0.015 g) were added into solution mixture and refluxed at 70^{o}C for 36 hours under argon atmosphere. 2-Bromothiophene (0.223 g, 1.368 mmol) and catalytic amount of extra catalyst were added and the solution mixture was stirred for 6 hours. Later on, trimethyl(thiophen-2-yl)stannane (1.02 g, 2.736 mmol) and catalytic amount of extra catalyst were added and stirred for 6 hours under same conditions. The reaction was cooled to room temperature and precipitated in cold methanol. Filtered mixture was purified by Soxhlett apparatus. The polymer **CoP3** was collected by chloroform and then the solvent was evaporated under vacuum. The solid residue was precipitated in cold methanol. Pure polymer was collected by vacuum filtration.

GPC: Mn: 5.6 kDa, Mw: 40.6 kDa, PDI: 7.25.

^{1}H NMR (400MHz, $CDCl_3$) δ (ppm): 7.9 (benzotriazole), 7.7 (quinoxaline), 7.3 (thiophene), 7.0 (benzene), 4.7 (N-CH_2), 2.2 (C-CH_2), 1.9-0.5 (pendant alkyl chains).

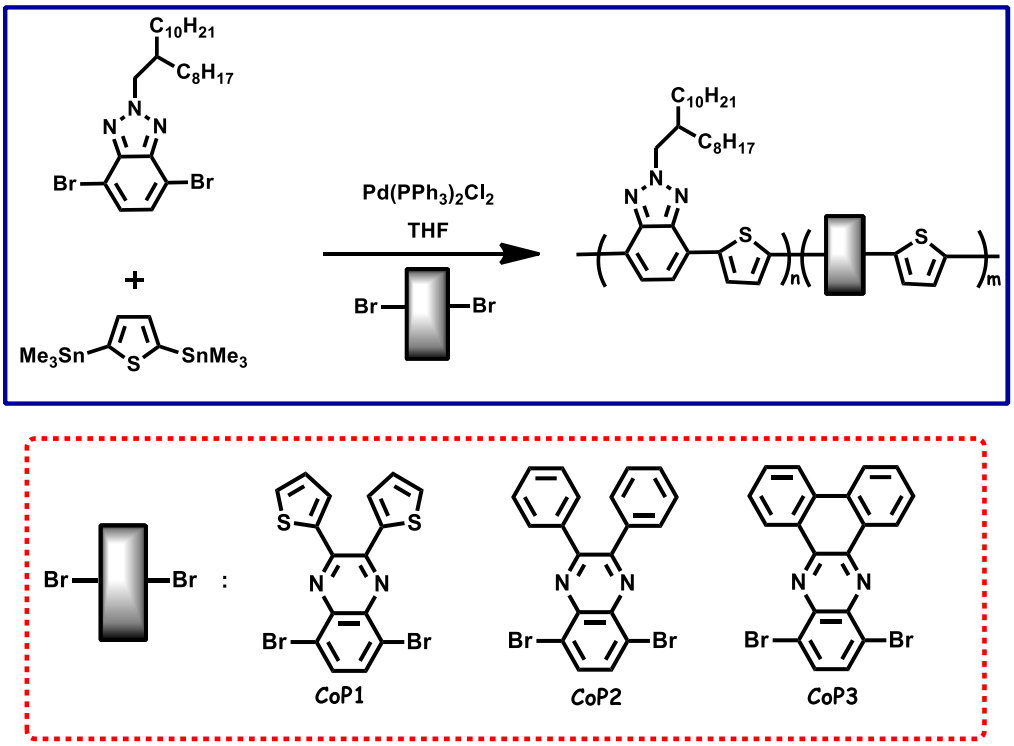

Figure 27. General synthetic pathway for all three copolymers CoP1, CoP2 and CoP3

2.4. Electrochemical Studies

Cyclic voltammetry (CV) studies were conducted to probe redox behaviors of polymers and to calculate HOMO and LUMO energy levels. In these studies, current density was measured as a function of applied potential. CV experiment was performed in three-electrode system in which platinum was utilized as the counter electrode (CE), the indium tin oxide (ITO) as working electrode (WE) and silver wire (calibrated to Fc/Fc^{+} redox couple) as reference electrode (RE). The main working principle of CV is based upon electrochemical reactions between polymer and immobile electrode via sweeping potential.

2.5. Spectroelectrochemical Studies

Spectroelectrochemical studies give deeper information about electrochromic properties of conjugated polymers by sweeping potential. The evolution of new intergap states such as polaron and bipolaron bands during doping process investigated by UV-Vis-NIR spectra as a function of applied electrode potential. Optical band gaps of copolymers were determined via maximum absorption wavelength onsets (λ_{max}^{onset}) in their neutral states. Color change was proved by sweeping potential.

2.6. Kinetic Studies

Kinetic studies were conducted to measure the transmittance change as a function of time between neutral and fully oxidized states of copolymers at their maximum absorption wavelengths under applied potential. Transmittance change, i.e. optical contrast, of copolymers at comparable wavelengths was recorded by UV-Vis-NIR spectrophotometer. The time needed to oxidize copolymer from its reduced state, i.e. switching time, was calculated by chronoamperometry.

2.7. Organic Solar Cell Studies

The BHJ organic solar cell device was fabricated with the structure of glass substrate/ITO/PEDOT:PSS/Polymer:$PC_{71}BM$/LiF/Al as the given order. ITO coated glass substrate was etched partially in order to take contacts and washed with toluene, detergent and water and later on with acetone and isopropyl alcohol in ultrasonic bath for 15minutes. ITO coated glass substrates were dried with N_2 gun. After the plasma cleaning (Harrick Plasma Cleaner), PEDOT:PSS was filtered through 0.45 μm PVDF syringe filter. PEDOT:PSS was coated onto the ITO surface at 5000 rpm for 1 minute by spin coating. To evaporate the water, substrates were dried at 130 °C for 15 minutes. Different ratios of polymer:$PC_{71}BM$ mixtures were prepared and filtered with 0.2 μm PTFE syringe filter. Filtered mixture was coated on PEDOT:PSS layer at different rpms by G3P-8 spin coater

in the glove-box system filled with nitrogen (O_2 concentration < 1 ppm and H_2O concentration < 1 ppm). A thin LiF (0.6 nm) and Al layer (100 nm) were evaporated through a shadow mask in sequence under vacuum of 10^{-6} mbar. The active area was 4 mm^2. Current density-voltage (J-V) characteristics were measured using a Keithley 2400 source meter under AM 1.5G irradiation (100 mV/cm^2) from a 1 kW Atlas Material Testing Solutions solar test 1200 solar simulator.

CHAPTER 3

3. RESULTS & DISCUSSION

3.1. Optical Properties of Copolymers

Optical properties of random copolymers in o-dichlorobenzene and in thin film are presented in **Figure 28** and summarized in **Table 1**. All of the three copolymers showed broad absorption in visible region. Copolymers have dual absorption peaks that could be assigned to π-π* transition and intermolecular charge transfer (ICT).[29]

Maximum absorption wavelength of **CoP1, CoP2** and **CoP3** in solution were observed at 585 nm, 586 nm and 546 nm respectively. Thin film absorption of **CoP1**, **CoP2** and **CoP3** revealed at 615 nm, 609 nm and 560 nm correspondingly. The maximum absorption spectra of the copolymers **CoP1**, **CoP2** and **CoP3** in the film were red shifted by 30-23-14 nm respectively compared with those in the solution resulted from decreased conformational freedom, aggregation or solvent-polymer interactions.[80] Among all, **CoP3** showed the least red-shift absorption (14 nm) which may result from less tendency to aggregation and less solvent-polymer chain interaction although it is expected more red shift compared to **CoP1** and **CoP2** due to its fused structure that increases the planarity and conjugation length.[28] This situation could be attributed to its low molecular weight.

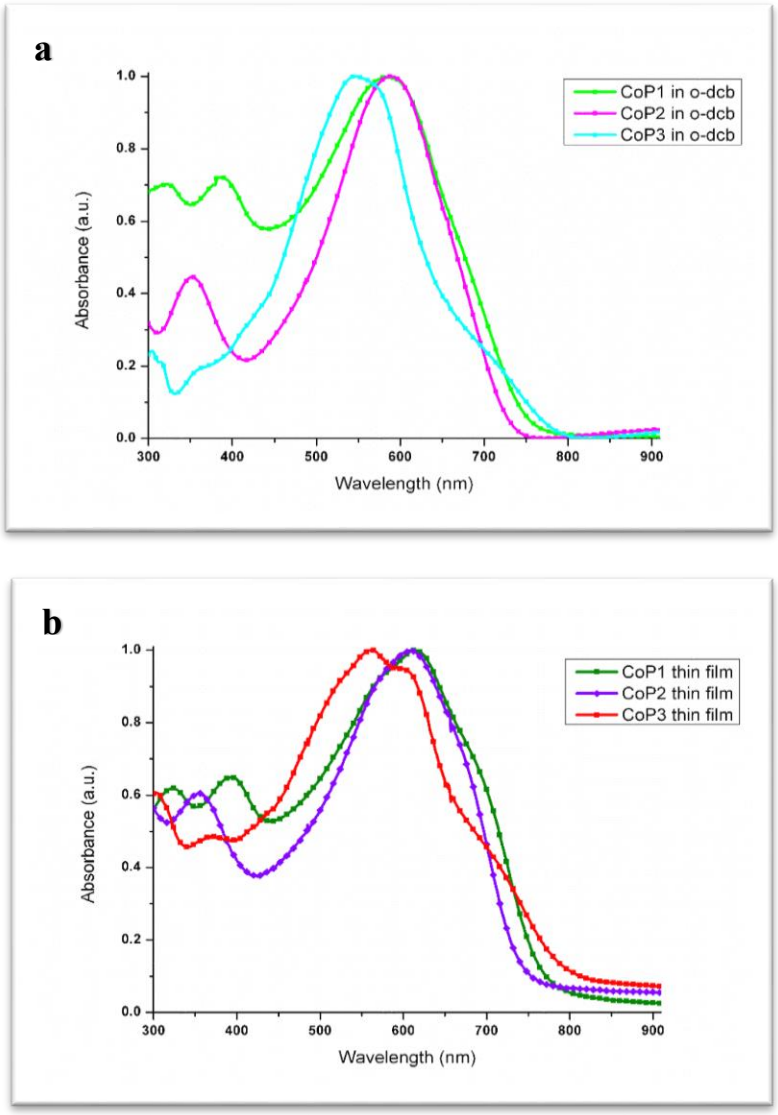

Figure 28. Absorption spectra of **CoP1**, **CoP2** and **CoP3** in (a) o-dichlorobenzene solution and (b) film states

Table 1. Absorption spectra of **CoP1**, **CoP2** and **CoP3** in o-dichlorobenzene solution and thin film

	Solution λ_{max} (nm)	**Thin Film λ_{max} (nm)**
CoP1	585	615
CoP2	586	609
CoP3	546	560

3.2. Electrochemical Properties of Copolymers

Cyclic voltammetry (CV) studies were performed to analyze oxidation and reduction potential of copolymers and to calculate HOMO and LUMO energy level from oxidation and reduction onset potentials. HOMO and LUMO energy levels were determined according to following equations:

$$HOMO = - (4.75+E_{ox}^{onset}+0.3)$$

$$E_g^{op} = HOMO- LUMO$$

Copolymers were dissolved in chloroform (5mg/mL) and spray coated on ITO surface. The potentials were scanned between -1.5 V and 2.0 V vs silver wire at 100 mV/s scan rate. Cyclic voltammograms are shown in **Figure 29** and electrochemical properties are summarized in **Table 2**. All copolymers have only p-doping character. Oxidation potential of **CoP1** was observed at 0.95 V with a dedoping peak at 0.50 V. Oxidation of **CoP2** was observed at higher potential than **CoP1** due to benzene ring and seen at 1.25 V/0.6 V. As expected oxidation potential of **CoP3** was 0.16 V lower than **CoP2** owing to its fused structure and seen at 0.97 V/0.90 V. HOMO energy levels of copolymers were found as -5.49, -5.40 and -5.59 eV for **CoP1, CoP2** and **CoP3** respectively. All copolymers have suitable HOMO energy level for polymer solar cell applications. Due to absence of n-type

dopable character, LUMO energy levels of copolymers were calculated from the difference of optical band gap and HOMO energy levels.

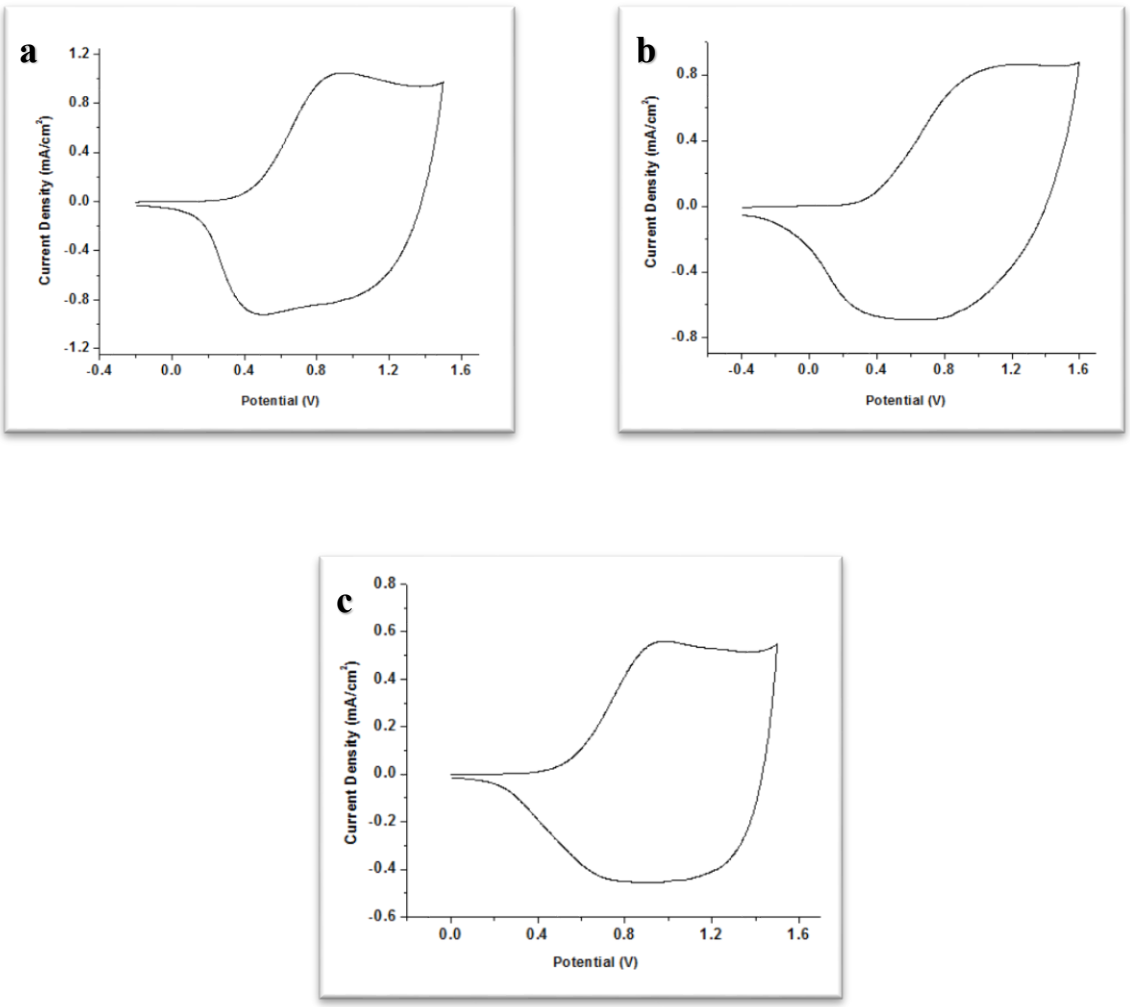

Figure 29. Single-scan cyclic voltammograms of copolymers films in 0.1 M $TBAPF_6$/ACN electrolyte solution (a) **CoP1** (b) **CoP2** (c) **CoP3**

The energy levels of materials used in OSC device fabrication were shown in **Figure 30.** According to HOMO levels of copolymers, **CoP1** shows the highest lying HOMO energy level as expected due to its lowest oxidation potential. Although high lying HOMO energy level provides lower V_{oc} value, it ensures low band gap energy which can harvest more

photons. Additionally, HOMO energy level is not the only criteria for obtaining low band gap polymers. LUMO energy level is also important for achieving low band gap and for reaching effective intermolecular charge transfer process between donor and acceptor units. In order to obtain better charge separation, LUMO energy level of donor polymer should be 0.3-0.5 eV higher than LUMO energy level of acceptor $PC_{71}BM$ (-4.2 eV).[29] According to LUMO energy levels of copolymers, the most effective charge transfer was seen in **CoP2** with -3.80 eV LUMO energy level.

Comparing the band gaps of copolymers, the lowest band gap was calculated for **CoP3** with 1.45 eV. Cyclization of the two dependent phenyl groups on quinoxaline unit exhibits increased planarity and conjugation length along the polymer backbone than the separated-phenyl rings involved in **CoP2** which resulted in lower band gap**.**[28,29] Thiophene rings gives **CoP1** more prolonged conjugation length than benzene rings locating in **CoP2**. Moreover, aromatic resonance stabilization of benzene is higher than thiophene unit which makes thiophene unit to adapt quinoid form more easily which lowers the band gap.[81] In consideration of the foregoing; the band gap of **CoP1** with 1.47 eV was found lower than the band gap of **CoP2** with 1.60 eV.

Table 2. Electrochemical Properties of **CoP1**, **CoP2** and **CoP3**

	CoP1	CoP2	CoP3
E_{ox}^{onset} (V)	0.44	0.35	0.54
E_{ox} (V)	0.95	1.25	0.97
E_{red} (V)	0.50	0.60	0.90
HOMO (eV)	-5.40	-5.49	-5.59
LUMO (eV)	-4.02	-3.80	-4.14
λ_{max} (nm)	615	609	560
λ_{max}^{onset} (nm)	844	775	855
E_g^{op} (eV)	1.47	1.60	1.45

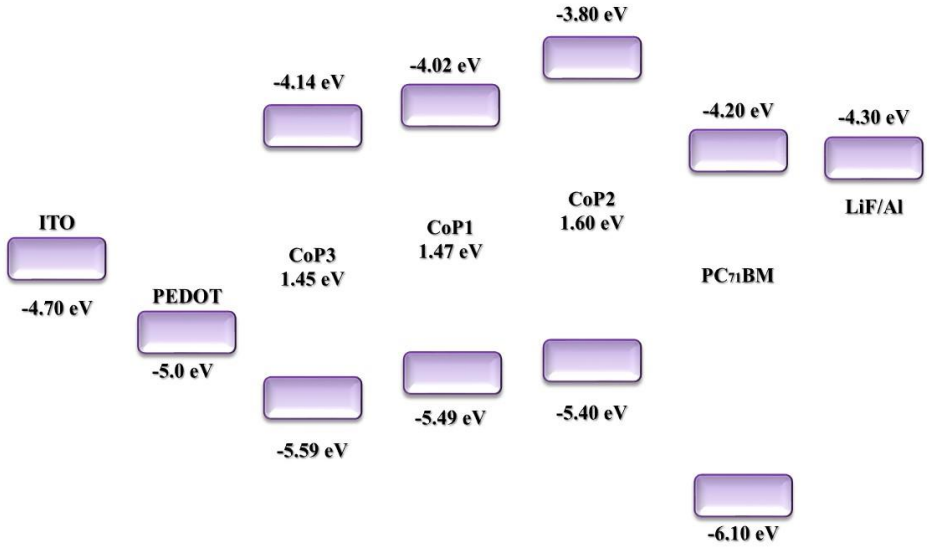

Figure 30. The energy levels of materials used in OSC device fabrication

3.3. Scan Rate Studies of Copolymers

The scan rate study gives information about anodic and cathodic current density values in given potential at different scan rates. According to Randles-Sevcik equation,

$$i_p = n^2F^2\nu A\Gamma / 4RT$$

The linear relationship between current density (i_p) and scan rate (ν) indicates that the mass transfer of anions in electrolyte solution to polymer surface is non-diffusion controlled. In other words, redox processes are controlled by mass transfer between anion layer constructed by electrolyte anion and oxidized polymer layer. As shown in **Figure 31,** the linear relationship was obtained for all copolymers **CoP1**, **CoP2** and **CoP3** and it was understood that electroactive redox processes of polymer films are reversible and non-diffusion controlled.

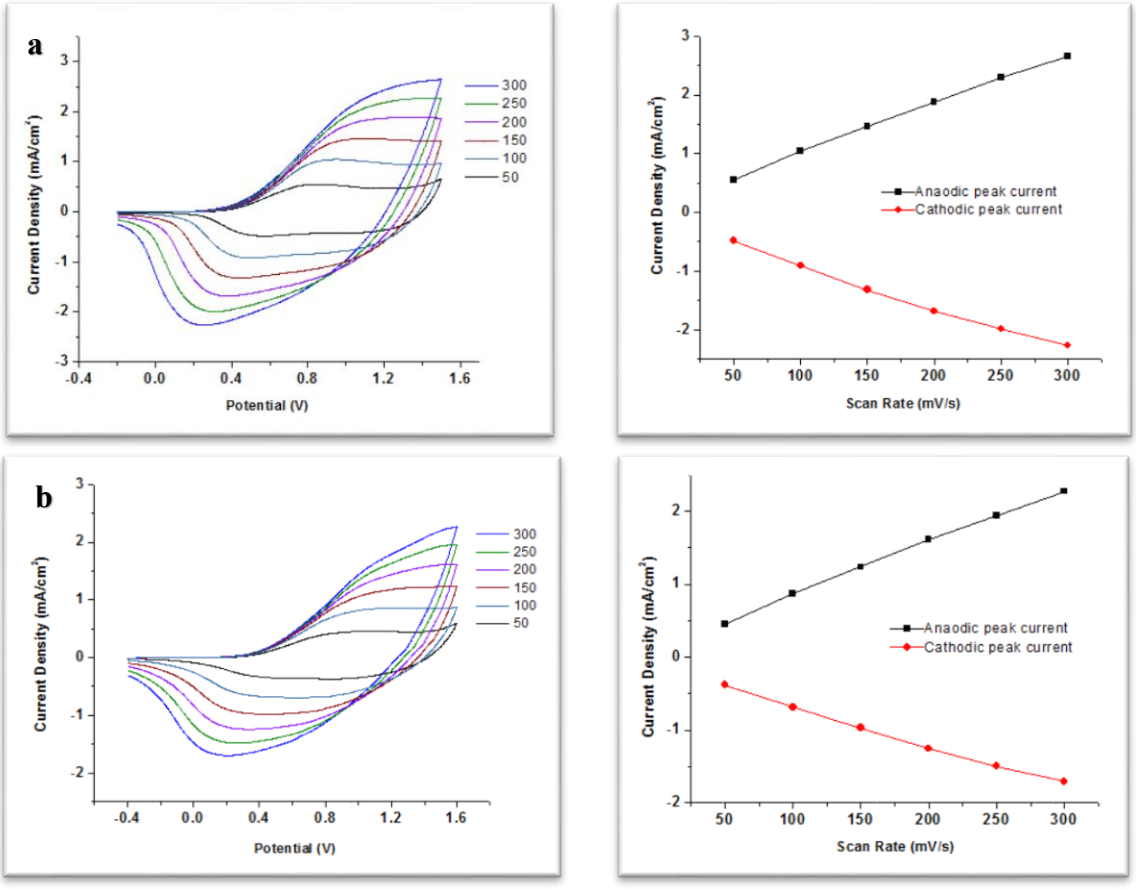

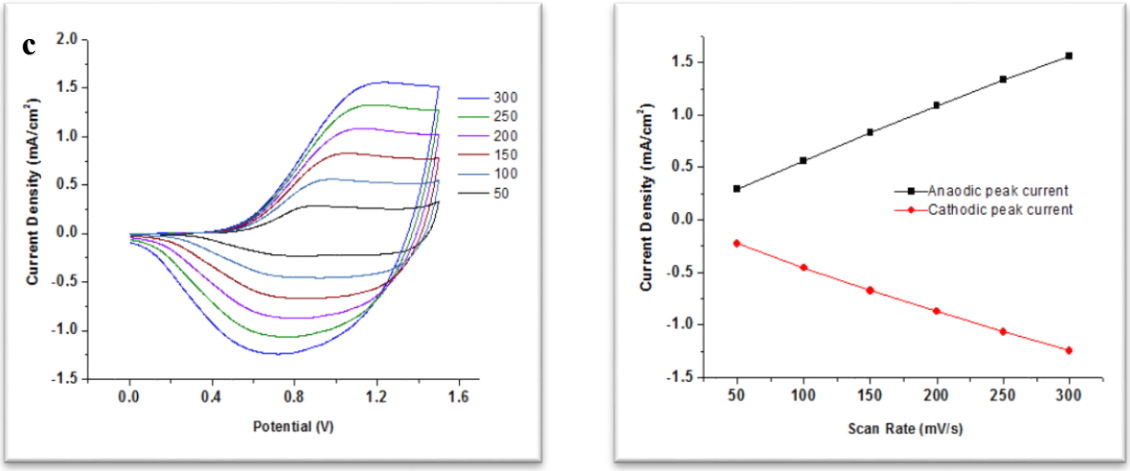

Figure 31. Scan rate studies in 0.1 M $TBAPF_6$/ACN at scan rates of 50, 100, 150, 200, 250 and 300 mV/s (a) **CoP1** (b) **CoP2** (c) **CoP3**

3.4. Spectroelectrochemical Properties of Copolymers

Spectroelectrochemical studies combine electrochemical and spectroscopic techniques to determine light absorption changes of copolymers as a function of wavelength through doping process. Copolymers dissolved in chloroform were coated on ITO and absorbance changes via applied potential were computed in UV-Vis-NIR spectra. All the measurements were done in 0.1 M $TBAPF_6$/ACN electrolyte solution with 0.2 V by 0.2 V increasing potential from 0.0 V to 1.6 V and the typical bipolaronic nature of the charge carriers was proven.

As shown in **Figure 32**, **CoP1** revealed a maximum absorption band (λ_{max}) at 615 nm with an onset of 844 nm. Optical band gap of **CoP1** was calculated as 1.47 eV from onset of λ_{max}. **CoP1** was observed as blackish blue (L: 53.492, a: 2.700, b: 4.39) in its neutral state. Upon oxidation, the color shifted to light purple-blue (L: 51.267, a: -3.963, b: 2.478) and light blue-green (L: 63.754, a: -4.699, b: 2.938). **CoP2** revealed a λ_{max} at 609 nm with an onset of 775 nm. Optical band gap of **CoP2** was calculated as 1.60 eV from the onset of λ_{max}. Optical band gap of **CoP2** was found higher than **CoP1** due to more aromatic benzene compound contribution instead of less aromatic thiophene ring. Electron donor

ability of thiophene is larger than benzene ring which increases HOMO energy level with increasing electron donor ability. Moreover, having thiophene ring on quinoxaline moiety indicates the prolonged conjugation length of copolymer. The neutral state of **CoP2** was observed as dark purple color (L: 38.376, a: 6.001, b: -12.786). Through increasing potential, **CoP2** became dark grey (L: 55.887, a: -3.718, b: 1.122) and later on sea green (L: 60.159, a: -10.083, b: 6.475). Lastly, λ_{max} was calculated at 560 nm with the absorption onset 855 nm for **CoP3**. Among all, the lowest optical band gap was achieved as 1.45 eV for **CoP3** due to its more rigid and planar structure than the others. Cyclization of two pendent phenyl rings on quinoxaline unit enhances the planarity along the chain backbone which increases the effective conjugation length.[29] **CoP3** was purple (L: 46.042, a: 13.222, b: -13.392) in its neutral state and through increasing voltage, it became lilac grey (L: 48.884, a: 5.384, b: -3.973) and sea green (L: 53.059, a: -8.978, b: 7.198). The lack of transparent color can be attributed to the tails of polaron peaks in the visible region of the spectrum.

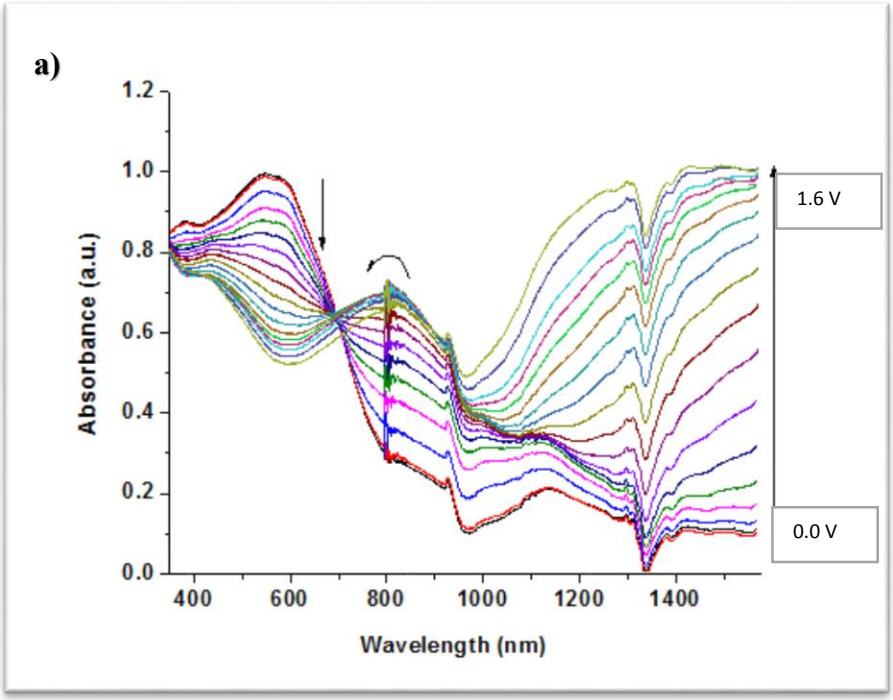

-0.2 V	1.0 V	1.5 V
		
L: 53.492 a:2.700 b:4.391	L: 51.267 a:-3.963 b:2.478	L: 63.754 a:-4.699 b:2.938

b)

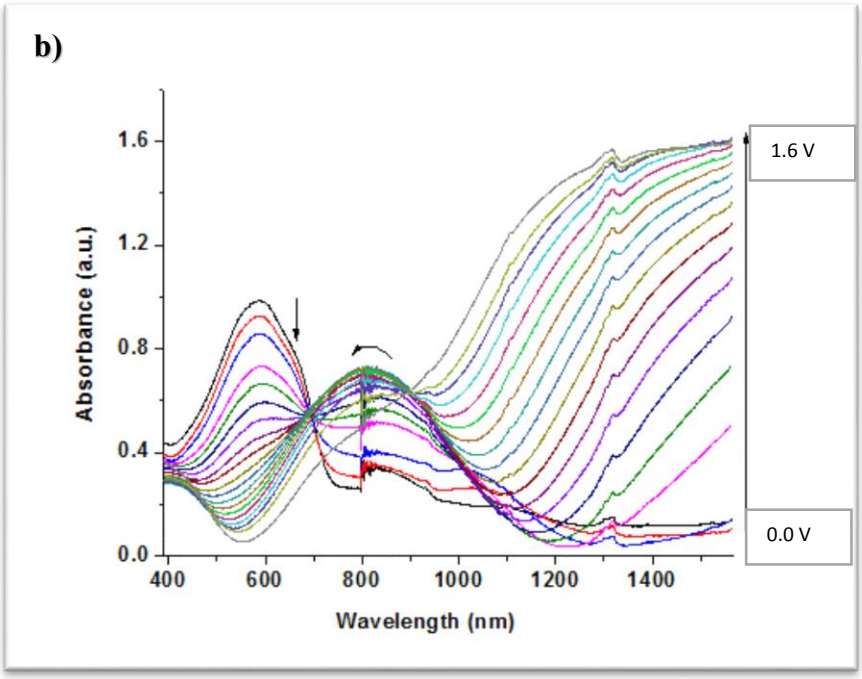

-0.4 V	**1.05 V**	**1.6 V**
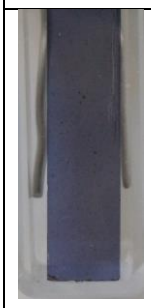		
L: 38.376 a:6.001 b:-12.786	L: 55.887 a:-3.718 b:1.122	L: 60.159 a:-10.083 b:6.475

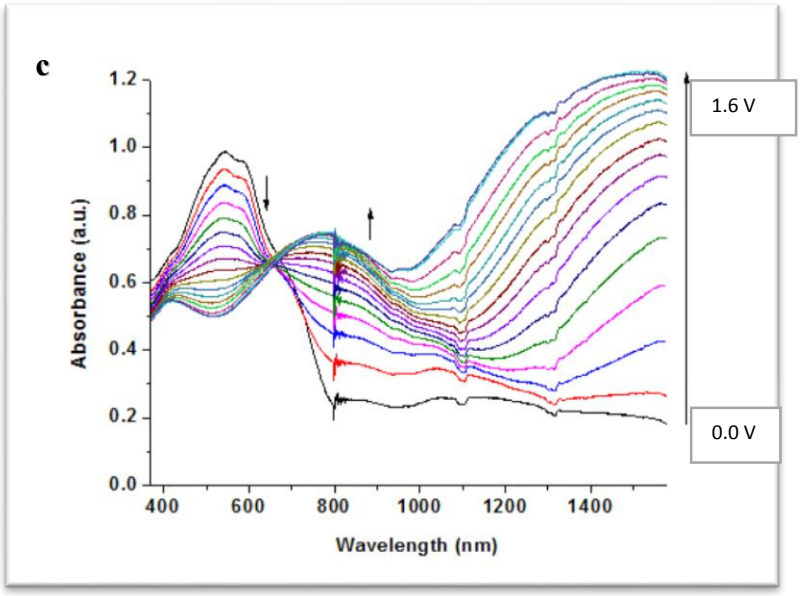

0.0 V	1.0 V	1.5 V
		
L: 46.042 a:13.222 b:-13.392	L: 48.884 a:5.384 b:-3.973	L: 53.059 a:-8.978 b:7.198

Figure 32. UV-Vis-NIR spectra of a) **CoP1** potential between -0.2 V and 1.5 V b) **CoP2** potential between -0.4 V and 1.6 V c) **CoP3** between 0.0 V and 1.5 V in 0.1 M $TBAPF_6$ / ACN electrolyte solution couple and the colors of corresponding polymers and their L, a and b values

3.5. Kinetic Studies of Copolymers

It's known that human eye is sensitive up to 95% of the full contrast. In this manner, the time needed for copolymers to switch from their neutral states to fully oxidized states, i.e. switching time, was defined at 95% of contrast value. Chronoamperometry studies were performed to determine the switching times of copolymers at their maximum absorption wavelengths and to monitor the percent transmittance changes as a function of time. During the experiment, percent transmittance changes were recorded by UV-Vis-NIR spectrophotometer between 0.0 V and 1.2 V potentials within 5 s time intervals (**Figure 33**). As summarized in **Table 3**, optical contrast values were found as 12% at 600 nm, 14% at 880 nm and 29% at 1500 nm for **CoP1** while switching times were calculated as 1.2, 1 and 0.7 s respectively. **CoP2** showed 35% at 580 nm, 29% at 830 nm and 60% at 1400 nm optical contrast values within 0.4, 1.0 and 0.4 s switching times which were the fastest switching time values among all. **CoP3** optical contrast values were found as 28% (545nm), 34% (860 nm) and 94% (1540 nm) along with 1.0, 1.5 and 0.8 s switching times. Kinetic studies indicated that except **CoP1**, **CoP2** and **CoP3** might be excellent candidates for near IR electrochromic device applications such as environmental heat gain and loss control systems in buildings, telecommunication windows or variable optical attenuators with their 60% and 94% optical contrast values respectively in NIR region.[82] Among all, **CoP3** achieved an outstanding 94% optical contrast with only 0.8 s switching time since it has more quinoid character.

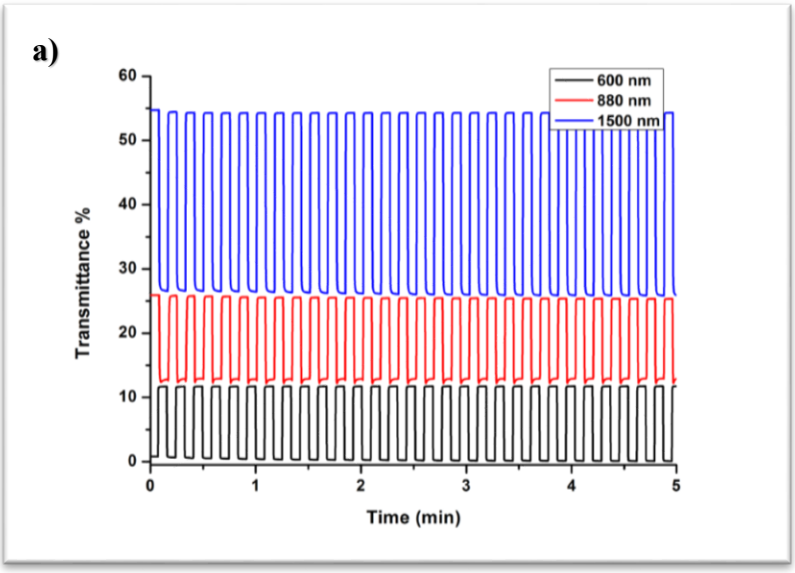
a)
600 nm
880 nm
1500 nm
Transmittance %
Time (min)
0
10
20
30
40
50
60
0
1
2
3
4
5

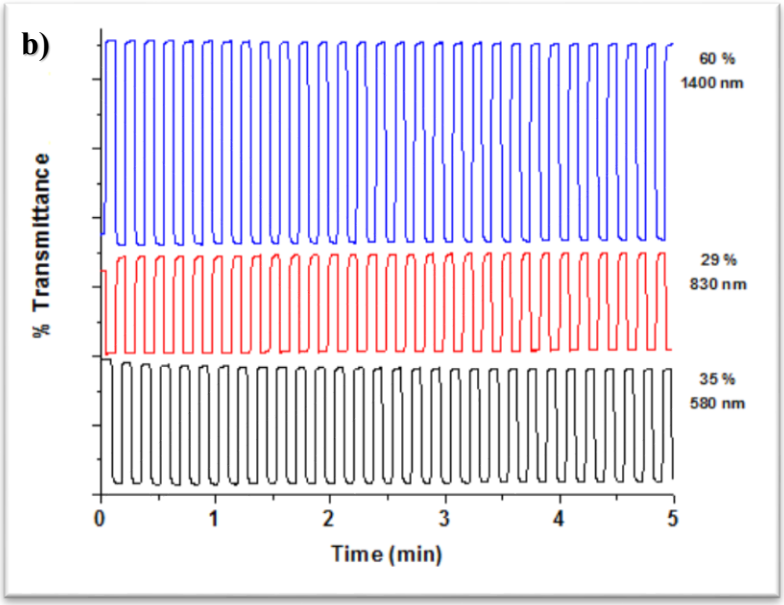
b)
60 %
1400 nm
29 %
830 nm
35 %
580 nm
% Transmittance
Time (min)
0
1
2
3
4
5

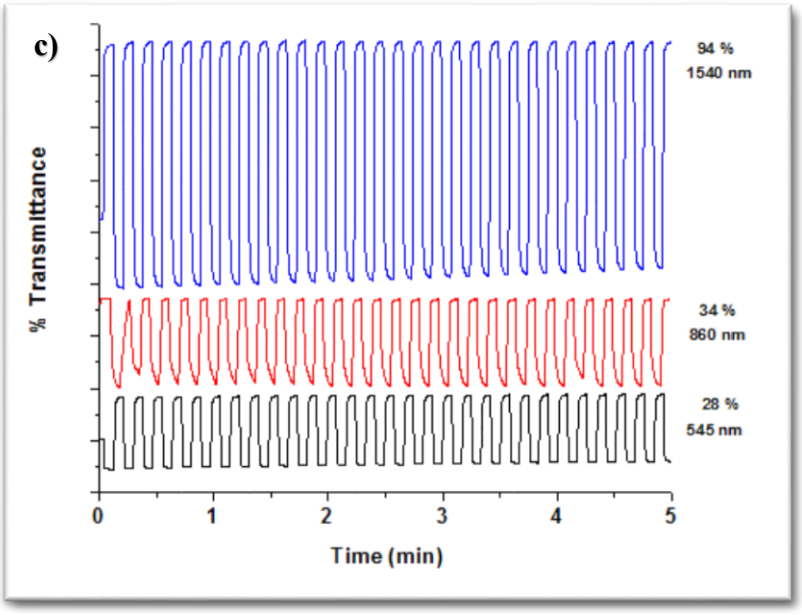

Figure 33. Percent transmittance change of (a) CoP1 (b) CoP2 (c) CoP3 in 0.1 M $TBAPF_6$ / ACN electrolyte solution at maximum wavelengths of copolymers

Table 3. Optical contrast and switching time values of **CoP1**, **CoP2** and **CoP3**

	Optical Contrast (%T)	**Switching Time (s)**
CoP1	**12% (600 nm)**	**1.2**
	14% (880 nm)	**1**
	29% (1500 nm)	**0.7**
CoP2	**35% (580 nm)**	**0.4**
	29% (830 nm)	**1.0**
	60% (1400 nm)	**0.4**
CoP3	**28% (545 nm)**	**1.0**
	34% (860 nm)	**1.5**
	94% (1540 nm)	**0.8**

3.6. Thermal Analyses of Copolymers

Thermogravimetry analyses of copolymers were performed via TGA and DSC under inert nitrogen atmosphere. Accordingly TGA results, 5% mass loss was observed at 420 °C for **CoP1,** at 400 °C for **CoP2** and at 430 °C for **CoP3**. 48.9%, 47.1%, 55 % mass loss was examined at 900 °C for **CoP1**, **CoP2** and **CoP3** respectively. Owing to rigid structures of copolymers, **CoP1**, **CoP2** and did not show glass-transition temperature (T_g). TGA and DSC analysis results were shown in **Appendix A**.

3.7. Organic Solar Cell Device Applications

Copolymers were utilized as the donor materials in the active layer of bulk heterojunction solar cell with the following device structure: ITO/PEDOT:PSS/ **CoP$_x$**+$PC_{71}BM$/LiF/Al. Polymer solar cell device studies were performed under 1.5 G illumination with 100 mW/cm^2. Current density-voltage (J-V) characteristics were investigated and power conversion efficiencies of copolymers were calculated as shown in the **Figure 34.** For all copolymers, different weight ratio of copolymer and $PC_{71}BM$ was chosen and spin coated on PEDOT-PSS coated ITO surface. Later, LiF was evaporated between active layer and cathode Al. LiF serves as the charge collection layer due to decreased energy barrier at the interface of active layer and cathode.[83,84] The best polymer solar cell performances for copolymers demonstrated power conversion efficiency (PCE) 2.13%, 1.77% and 0.95% for **CoP1**, **CoP2** and **CoP3** respectively as summarized in **Table 4**. The highest PCE value was obtained for **CoP1** since J_{sc} of **CoP1** showed the highest value of 8.07 mA/cm^2 due to its broader absorption of the solar spectrum. In contrast, the lowest PCE value was attained for **CoP3** in despite of its lowest band gap and the most planar structure among all. This might be due to lower molecular weight or narrow absorption of solar spectrum in the range of 570-750 nm which resulted in low J_{sc}. In addition to those effects, morphology and choice of the solvent might attributed the difference between PCE values of copolymers. V_{oc} is theoretically the difference between HOMO energy level of donor (CoP_x) and LUMO energy level of acceptor ($PC_{71}BM$). While theoretically V_{oc} values were high for **CoP1**, **CoP2** and **CoP3**, experimentally they showed lower results. V_{oc} losses might be attributed to charge transfer state complexes, poor dielectric properties or disorder-induced varieties in the hole/electron quasi-Fermi levels.[85] For all copolymers, V_{oc} values was observed in the range of 0.52-0.57 V.

By using incident photon to current efficiency (IPCE) method, the ratio of number of charges collected by electrodes to the number of incident photons was obtained for polymer solar cells which were prepared by 1:2 **CoP**1:$PC_{71}BM$, 1:3 **CoP2**:$PC_{71}BM$ and 1:3 **CoP3**:$PC_{71}BM$ weight ratio (**Figure 35**). The measurements were done in the range

of 300-1000 nm using monochromic light. The maximum IPCE for **CoP1** was found as 38.33%, 23.24% for **CoP2** and 10.47% for **CoP3**. As a result, IPCE absorption spectrum was revealed features similar to UV-Vis absorption spectrum of CoP_x:$PC_{71}BM$ blend (**Figure 36**) as expected.

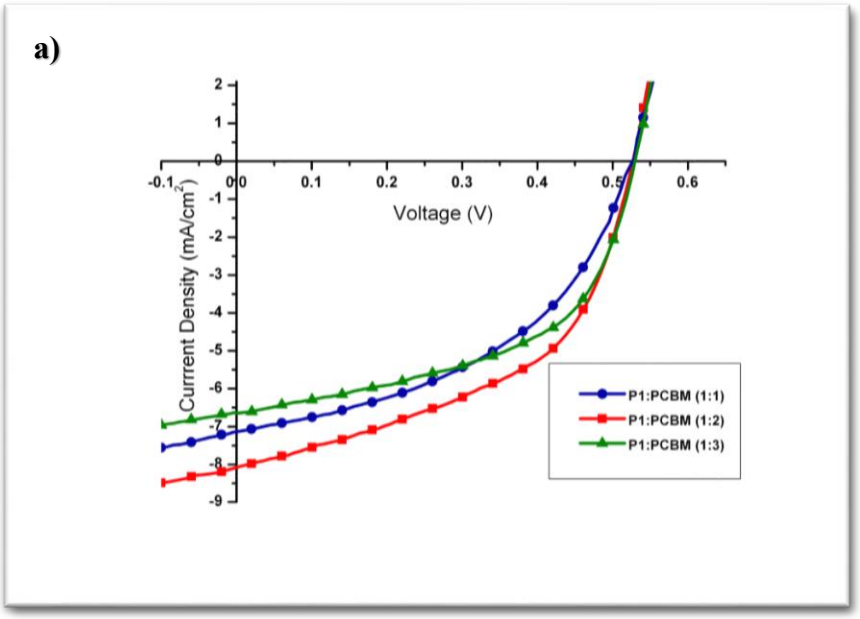

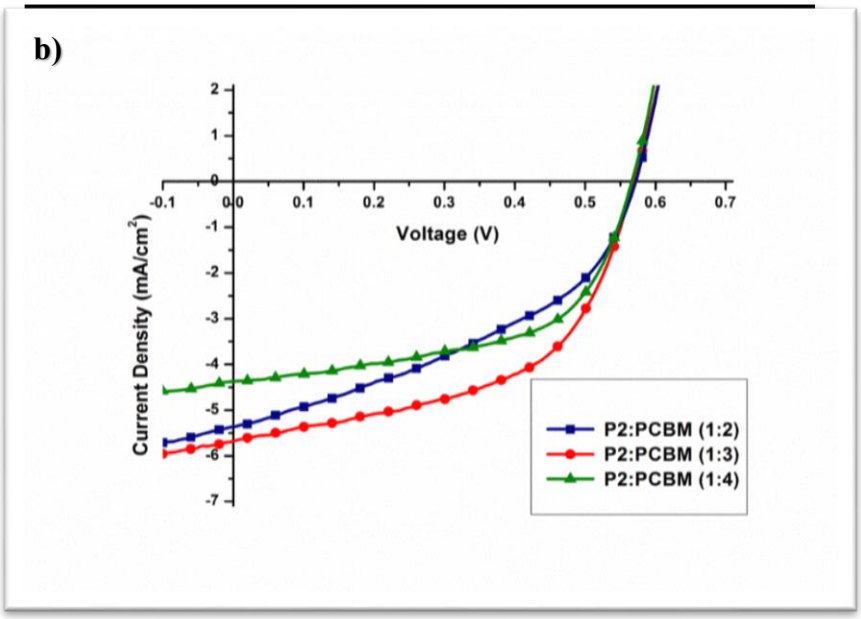

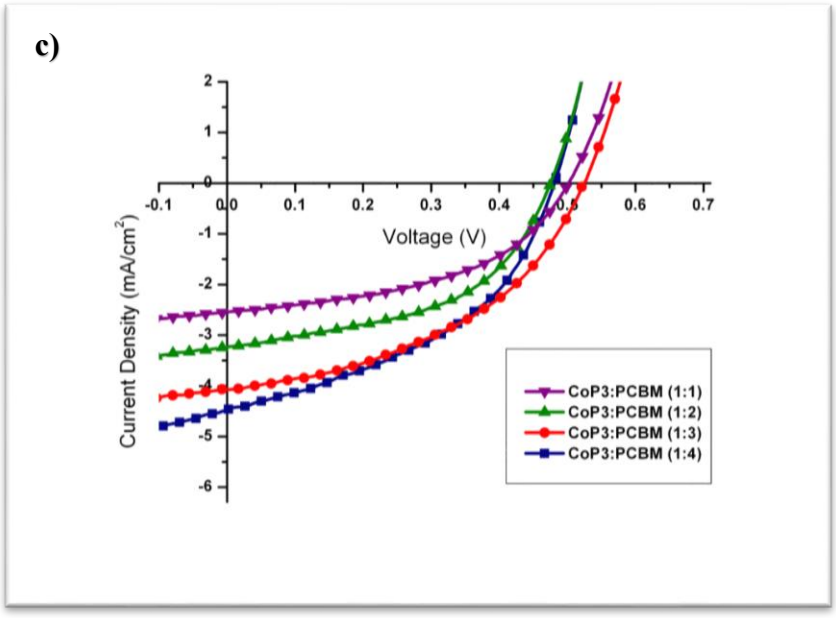

Figure 34. Current density-voltage (J-V) characteristics of (a) **CoP1** (b) **CoP2** and (c) **CoP3**

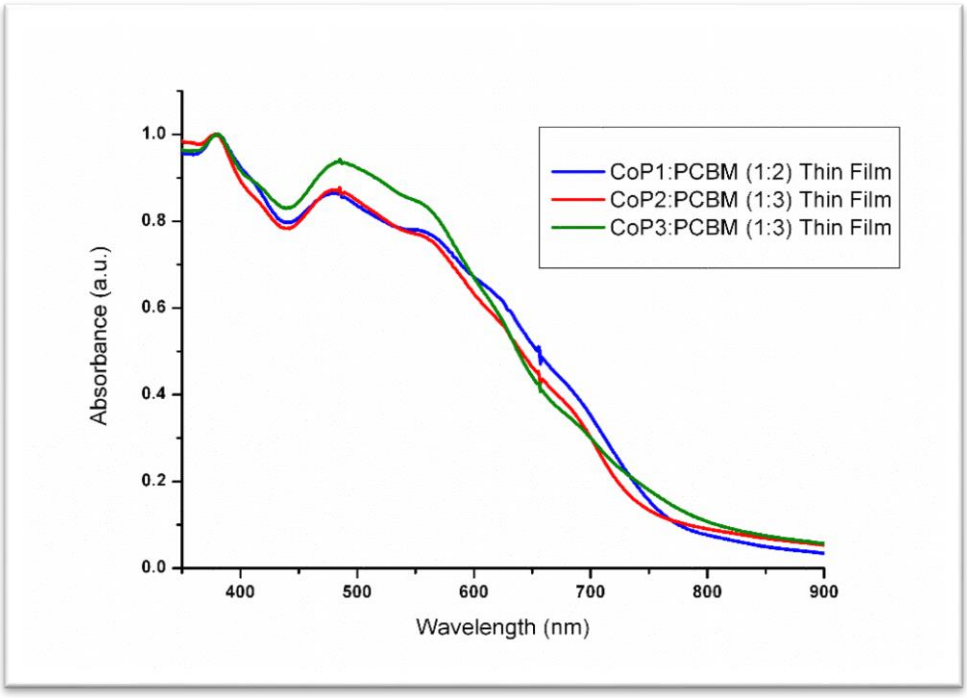

Figure 35. Normalized film absorbance spectra for polymer and PCBM mixtures

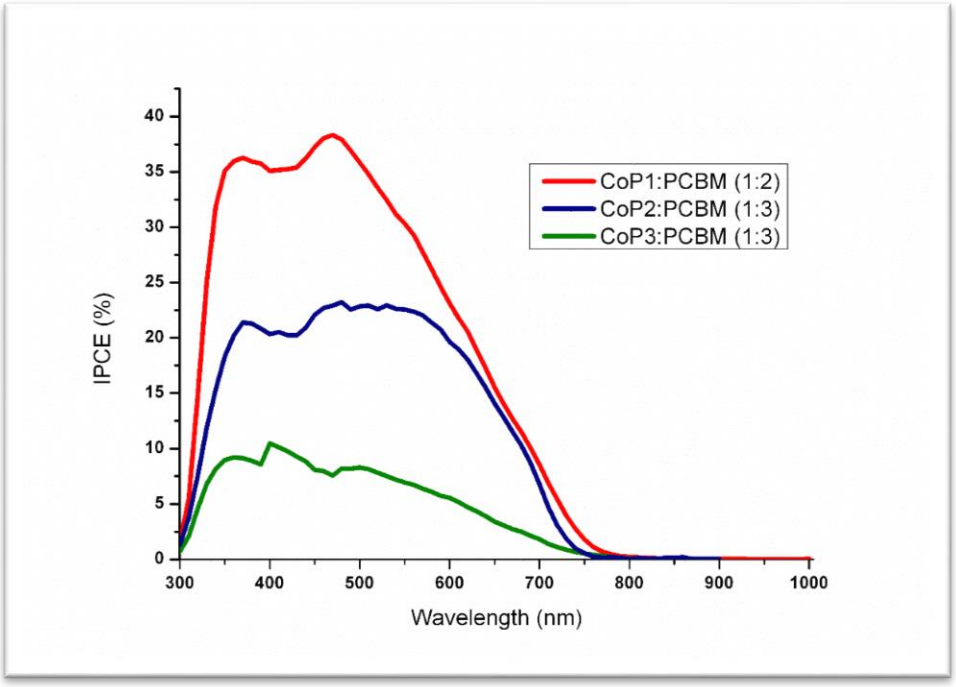

Figure 36. IPCE values of polymer solar cell device

Hole mobility values of **CoP1**, **CoP2** and **CoP3** were investigated from the current-voltage characteristics (J-V curve) of corresponding copolymers under dark via space charge limited current model. Hole mobility values of copolymers were calculated with Child's Law:

$$J_{\mathrm{SCLC}} = \frac{9}{8}\varepsilon_0\ \theta\ \varepsilon_r \mu \frac{V^2}{L^3}$$

Where J is the current, μ is the mobility of charge carriers, V is the applied voltage, L is the thickness of the copolymer, ε_0 is the dielectric permittivity of vacuum, ε_r is the dielectric permittivity of polymer and Θ is the trap-limiting parameter.

SCLC graphs were shown in **Figure 37** and summarized in **Table 4**. The average hole mobility values for CoP_x+$PC_{71}BM$ blends were correlated with the polymer organic solar cell device performance. The highest hole mobility value was found as 1.49×10^{-3} $cm^2/V.s$ for **CoP1** with the highest efficiency of 2.13%. As expected the lowest mobility value was found as 8.50×10^{-4} $cm^2/V.s$ for **CoP3** with the lowest efficiency of 0.95%.

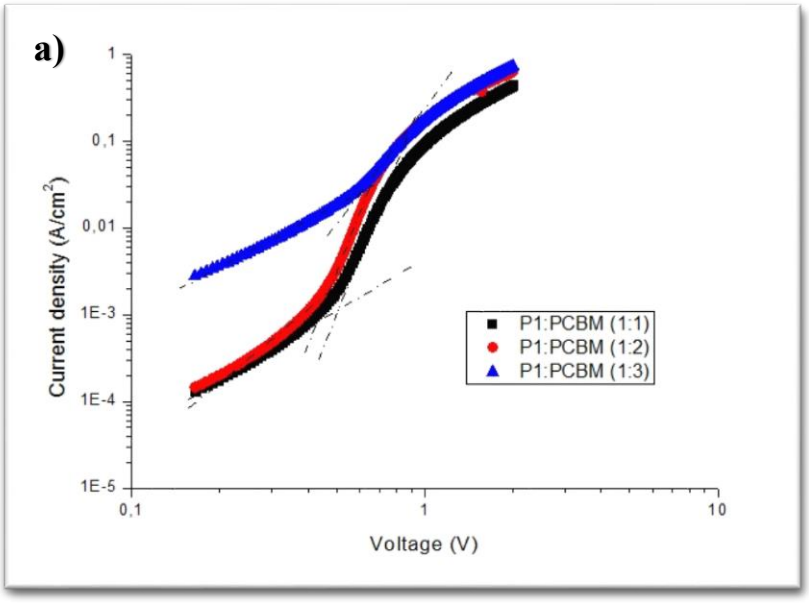

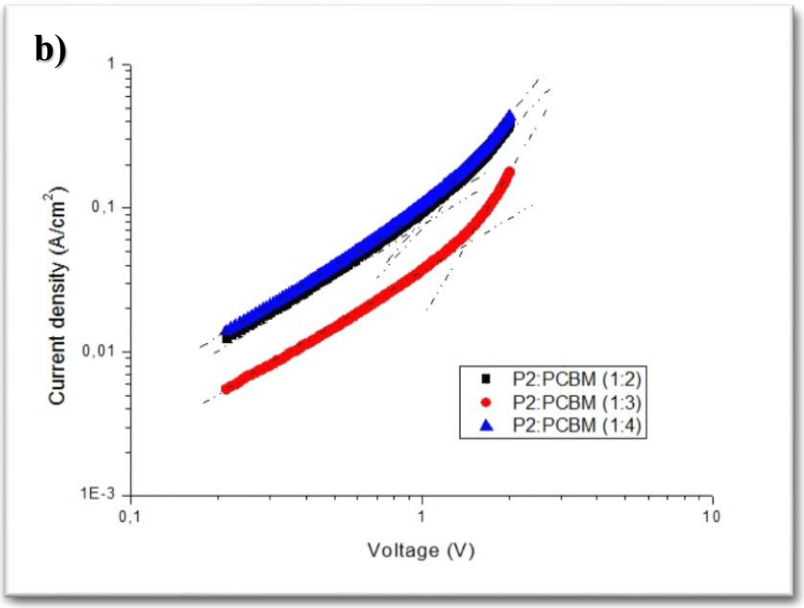

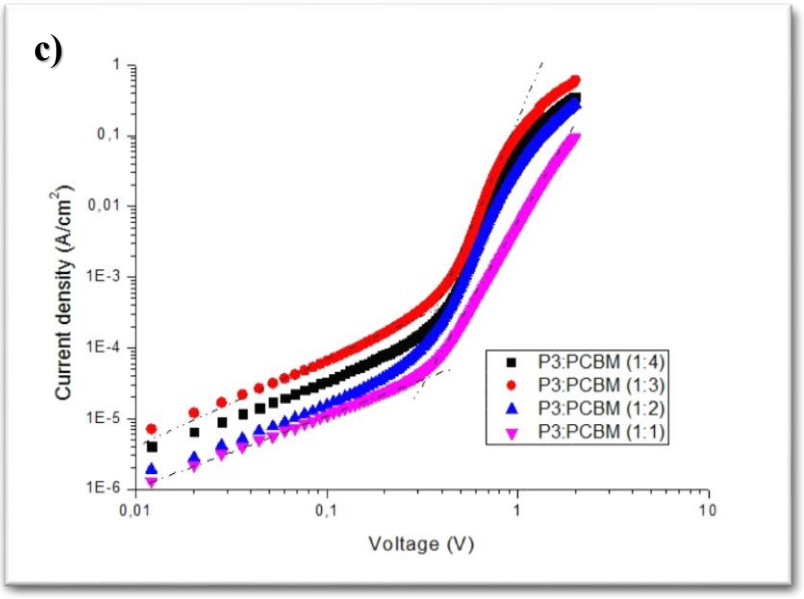

Figure 37. Logarithmic J-V curve for (a) **CoP1** (b)**CoP2** and (c) **CoP3**

Table 4. Summary of polymer solar cell device studies

Polymer	Polymer $PC_{71}BM$ ratio	Thickness (nm)	V_{oc} (V)	J_{sc} (mA/cm^2)	μ ($cm^2/V.s$)	FF (%)	η (%)
CoP1	1:1	90	0.53	7.14	$1.06x10^{-3}$	46	1.74
	1:2	95	0.53	8.07	$1.49x10^{-3}$	50	2.13
	1:3	100	0.53	6.63	$1.29x10^{-3}$	53	1.86
CoP2	1:2	95	0.57	5.40	$3.13x10^{-4}$	44	1.35
	1:3	100	0.57	5.57	$4.34x10^{-4}$	56	1.77
	1:4	105	0.57	4.40	$3.97x10^{-4}$	55	1.38
CoP3	1:1	80	0.50	2.54	$3.86x10^{-5}$	47	0.60
	1:2	85	0.48	3.22	$2.97x10^{-4}$	50	0.77
	1:3	90	0.52	4.07	$8.50x10^{-4}$	45	0.95
	1:4	95	0.48	4.50	$6.61x10^{-4}$	44	0.95

CHAPTER 4

4. CONCLUSIONS

In this study, in order to investigate the effects of substituents of the quinoxaline-based conjugated polymers, D-A type three conjugated copolymers **CoP1**, **CoP2** and **CoP3** were synthesized via Stille coupling. Solubility of polymers were enhanced by substituting 2-octyl-dodecyl unit on the 2-position of the BTz moiety. Synthesized copolymers were used in the active layer of bulk heterojunction polymer solar cell devices. Electrochemical, spectroelectrochemical and kinetic studies were conducted to probe electrochemical and electrochromic properties of copolymers.

Electrochemical studies represented that all copolymers had p-doping character. **CoP2** had the most electron deficient nature with the highest oxidation potential. From spectroelectrochemical studies, the highest optical band gap was calculated for **CoP2** with 1.60 eV. In contrast, **CoP3** showed the lowest optical band gap (1.45 eV) among all due to its more fused and rigid structure which increases the planarity and conjugation length. Moreover, all copolymers presented full visible region absorption with multichromism due to the extension of polaron band into visible region. Electrochemical and optical experiments revealed that copolymers are applicable for polymer solar cell applications owing to their proper HOMO and LUMO energy levels, low band gaps and broad range absorption of visible spectrum. Kinetic studies indicated that **CoP2** and **CoP3** might be excellent candidates for NIR electrochromic device applications owing to their 60% and 94% optical contrast values respectively in NIR region with <1 s switching times.

Bulk heterojunction polymer solar cell device fabrication were performed with three copolymers as donor units in the active layer. Among all, the highest PCE was reported as 2.13 % for **CoP1** with high J_{sc} value (8.07 mA/cm^2**)**, moderate V_{oc} value (0.53 V), low FF value (50%) and sufficient IPCE value (38.33 %). From SCLC mobility measurements, the highest hole mobility was calculated as 1.49×10^{-3} cm^2/V.s for **CoP1**. **CoP2** also exhibited good PCE value as 1.77 %. The lowest PCE value was computed as 0.95 % for **CoP3**. Decrease in mobility of **CoP3** could be related to the low molecular weight of CoP3 since intermolecular charge-hopping enhanced by the length of the polymer chain that is determined by molecular weight.

5. REFERENCES

1. IUPAC. Compendium of Chemical Terminology, 2006, http://goldbook.iupac.org/C01267.html [last accessed on August 2015]
2. Facchetti, Chem Matter, 2011, 23, 733–758.
3. G. Inzelt, Conducting Polymers, 2012, Springer-Verlag Berlin Heidelberg.
4. D. Baran, A. Balan, S. Celebi, B. M. Esteban, H. Neugebauer, N. S. Sariciftci, L. Toppare, Chem. Mater., 2010, 22, 2978–2987.
5. K. Lee, G. A. Sotzing, Chem. Commun., 2013, 49, 5192.
6. A. Balan, D. Baran, G. Gunbas, A. Durmus, F. Ozyurta, L. Toppare, Chem. Commun., 2009, 6768.
7. Y. Qi, Encyclopedia of Nanotechnology, 2012, pp 583-587
8. B. A. Gregg, R. A. Cornier, J. Am. Chem. Soc., 2001, 123, 795-7960
9. B. Lüssem, M. Riede, K. Leo, Phys. Status Solidi A, 2013, 210, No. 1.
10. J. M. Nunzi, C.R. Physique, 2002, 3, 523-542.
11. H. A. M. van Mullekom, J. A. J. M. Vekemans, E. E. Havinga, E. W. Meijer., Mater. Sci. Eng., 2001, (32)1-40.
12. T. A. Skotheim, R. L. Elsenbaumer, J. R. Reynolds, Handbook of Conducting Polymers, 2nd edn, 1998, Marcel Dekker Inc., New York.
13. S. J. Higgins. Chem. Soc. Rev., 1997, (26) 247.
14. I. Schwendeman, PhD Thesis, University of Florida, 2002.
15. F. Wudl, M. Kobayashi, A. J. Heeger, J. Org. Chem., 1984, 49, 3382.
16. Y. J. Cheng, S. H. Yang, C. S. Hsu, Chem. Rev., 2009, 109 (11), 5868-5923.
17. C. Winder and N. S. Sariciftci, J. Mater. Chem., 2004, 14, 1077-1086.
18. R. J. Waltman, J. Bargon and A. F. Diaz, J. Phys. Chem., 1983, 87(8), 1459-1463.
19. K. Shimamura, F.E. Karasz, J.A. Hirsch, J.C. Chien, Macromol. Chem. Rapid Commun., 1981, 2, 443.

20. J. Roncali, R. Garreau, A. Yassar, P. Marque, F. Garnier and M. Lemaire, J. Phys. Chem., 1997, 91 (27), 6706-6714.
21. R. D. McCullough, R. D. Lowe, M. Jayaraman and D. L. Anderson, J. Org. Chem., 1993, 85, 904.
22. H. Zhou, L. Yang and W. You, Macromolecules, 2012, 45, 607-632.
23. H. A. M. Mullekom, J.A.J.M. Vekemans, E.E. Havinga and E.W. Meijer., Mater. Sci. Eng., 2001, R32,1.
24. E. E. Havinga, W. Hoeve, H. Wynberg, Polym. Bull., 1992, 29, 119–126.
25. E. E. Havinga, W. Hoeve, H. Wynberg, Synth. Met., 1993, 55, 299–306.
26. T. Kanbara, T. Yamamoto, Chem. Lett, 1993, 22, 419.
27. C.A. Thomas, K. Zong, K.A. Abboud, P.J. Steel and J.R. Reynolds, J. Am. Chem. Soc., 2004, 126, 50, 16440.
28. H. J. Song, J. Y. Lee, E. J. Lee, D. K. Moon, Eur Polym J, 2013, 49, 3261-3270.
29. Y. Lee, Y. M. Nam, W. H. Jo, J. Mater. Chem., 2011, 21, 8583.
30. T. Yamamoto, K. Sugiyama, T. Kanbara, H. Hayashi, H. Etori, Macromol. Chem. Phys., 1998, 199, 1807.
31. A. Tanimoto, T. Yamamoto, Macromolecules, 2006, 39, 3546.
32. A. Balan, G. Gunbas, A. Durmus and L. Toppare, Chem. Mater., 2008, 20, 7510.
33. W. W. H. Wong, J. Subbiah, S. R. Puniredd, W. Pisula, D. J. Jones and A. B. Holmes, Polym. Chem., 2014, 5, 1258-1263.
34. A. Tanimoto and T. Yamamoto, Adv. Synth. Catal., 2004, 346, 1818-1823
35. M. R. Detty, Chemistry of Heterocyclic Compounds, 1994, Willey, p.112.
36. Y. Liang, L. Yu, Polymer Reviews, 2010, 50:454–473.
37. P. R. Somani, S. Radhakrishnan, Mater. Chem. and Phys., 2002, 77, 117.
38. C. L. Gaupp, J. R. Reynolds, Macromolecules, 2003, 36, 6305.
39. International Tungsten Industry Association, 2013, http://www.itia.info/assets/files/newsletters/Newsletter_2013_06.pdf [Last accessed on September 2015].

40. J.H. Burroughes, D.D.C. Bradley, A.R Brown, R.N Marks, K. Mackay, R.H Friend, P.L Burn, A.B Holmes, Nature, 1990, 347, 539.
41. R. Prakash, A. Somani, S. Radhakrishnan, Mater Chem Phys, 2002, (77) 117–133.
42. A. A. Avni, P. H. Aubert, B. C. Thompson, I. Schwendeman, C. L. Gaupp, J. Hwang, N. J. Pinto, D. B. Tanner, A. G. MacDiarmid, J. R. Reynolds, Chem. Mater., 2004, 16, 4401-4412.
43. M. A. Chad, L. D. Aubrey, J. R. Reynolds, Chem. Mater., 2011, (23) 397–415.
44. [a] J. Roncali, Chem. Rev., 1997, 97, 173, [b] J. Roncali, Macromol. Rapid Commun., 2007, 28, 1761.
45. A. A. Argun, PhD Thesis, University of Florida, 2004.
46. R. N. Marks et al., J. Phys.: Condens. Matter, 1994, 6, 1379.
47. T. L. Benanti, D. Venkataraman, Photosynth. Res., 2006, 87, 73-81.
48. T. M. Clarke, J. R. Durrant, Chem. Rev., 2010, 110, 6736-6767.
49. S. Gunes, H. Neugebauer, N. S. Sariciftci, Chem. Rev., 2007, 107, 1324-1338.
50. W. C. H. Choy, Springer-Verlag London, 2013.
51. SNE Research, 2012, http://www.sneresearch.com/eng/info/show.php?c_id=4561&pg=2&s_sort=2&sub_cat=&s_type=&s_word, [last accessed on August 2015].
52. A. Durmus, G. E. Gunbas, L. Toppare, Chem. Mater., 2007, 19, 6247-6251.
53. C. W. Tang, Appl. Phys. Lett., 1986, 48, 183.
54. J. M. Halls, Appl. Phys. Lett., 1986, 68, 3120.
55. L. S. Roman, L. A. A. Patterson, O. J. Inganas, J. Appl. Phys., 1999, 86, 487.
56. M. Theander, O. Phys. Rev., 2000, 61, 12957.
57. S. R. Forrest, MRS Bulletin, 2005, 30, 28.
58. P. W. M. Blom, V. D. Mihailetchi, L. J. A. Koster and D. E Markov, Adv. Mater., 2007, 19, 1551-1566.
59. J. L. Bredas, J. E. Norton, J. Cornil and V. Coropceanu, Acc. Chem. Res., 2009, 42 (11), 1691-1699.
60. A. Moliton ad J. M. Nunzi, Polym. Int., 2006, 55, 583-600.

61. P. Heremans, V. I. Arkhipov, H. Bassler, Appl. Phys. Lett., 2003, 82, 4605.
62. M. C. Scharber, D. Mühlbacher, M. Koppe, P. Denk, C. Waldauf, A. J. Heeger and C. J. Brabec, Adv. Mater., 2006, 18, 789-794
63. N. Miyaura and A. Suzuki, Chem. Rev., 1995, 95, 2457-2483
64. X. Yang and A. Uddin, Renew. Sust. Energ. Rev, 2014, 30, 324-336
65. E. Bundgaard and F. C. Krebs, Renew. Sust. Energ. Rev, 2007, 91, 954-985
66. E. Bundgaard, S. E. Shaheen, F. C. Krebs and D. S. Ginley, Sol. Energ. Mat. Sol. C., 2007, 91, 1631-1637
67. S. H. Park, A. Roy, S. Beaupre, S. Cho, N. Coates, J. S. Moon, D. Moses, M. Leclerc, K. Lee and A. J. Heeger, Nat. Photonics, 2009, 3, 297.
68. G. Dennler, M. C. Scharber and C. J. Brabec, Adv. Mater., 21, 2009, 1323-1338
69. V. D. Mihailetchi, H. Xie, B. de Boer, L. J. A. Koster and P. W. M. Blom, Adv. Funct. Mater., 16, 2006, 699-708
70. C. J. Brabec, A. Cravino, D. Meissner, N. S. Sariciftci, T. Fromherz, M. T. Rispens, L. Sanchez and J. C. Hummelen, Adv. Funct. Mater., 11 (5), 2001, 374-380
71. R. Gottschalg, T.R. Betts, D.G. Infield, and M.J. Kearney, Sol. Energ. Mat. Sol. C., 2005, 85,415-428.
72. S. C. Cevher, N. A. Unlu, A. C. Ozelcaglayan, D. H. Apaydin, Y. A. Udum, L. Toppare, A. Cirpan, J. Polym. Sci. A Polym. Chem., 2013, 51, 1933-1941.
73. J. L. Banal, J. Subbiah, H. Graham, J. K. Lee, K. P. Ghiggino, W. W. H. Wong, Polym. Chem., 2013, 4, 1077.
74. W. W. H. Wong, J. Subbiah, S. R. Puniredd, W. Pisula, D. J. Jones, A. B. Holmes, Polym. Chem., 2014, 5, 1258-1263.
75. S. C. Price, A. C. Stuart, L. Yang, H. Zhou and W. You, J. Am. Chem. Soc., 2011, **133**, 4625–4631.
76. E. Wang, L. Hou, Z. Wang, S. Hellstrom, F. Zhang, O. Inganas, M. R. Andersson, Adv. Mater., 2010, 22, 5240.

77. M.-H. Lai, C.-C. Chueh, W.-C. Chen, J.-L. Wu and F.-C. Chen, J. Polym. Sci., Part A: Polym. Chem., 2009, **47**, 973.
78. Y.-L. Yang, Y.-H. Lee, C.-J. Chang, A.-J. Lu, W.-C. Hsu, L. Wang, M.-K. Leung and C.-A. Dai, J. Polym. Sci., Part A: Polym. Chem., 2010, **48**, 1607.
79. Y. Zhang, J. Zou, K-S. Chen, D. F. Zeigler, Y. Sun, Chem. Mater., 2011, 23 (9), 2289-91.
80. G. Hizalan, A. Balan, D. Baran, L. Toppare, J. Mater. Chem., 2011, 21, 1804
81. Z. Gao, B. Qu, H. Wu, C. Gao, H. Yang, L. Zhang, L. Xiao, Z. Chen, Q. Gong, J. Appl. Polym. Sci., 2014.
82. K. Aydemir, S. Tarkuc, A. Durmus, G. E. Gunbas, and L. Toppare, Polymer, 2008, 49, 2029–2032.
83. C. J. Brabec, S. E. Shaheen, C. Winder, N. S. Sariciftci, and P.Denk, Appl. Phys. Lett., 2002, 80, 1288–1290.
84. H. J. Park, Y. Lee, J. W.Jo, and W. H.Jo, Polym. Chem., 2012, 3, 2928–2932.
85. J. J. Intemann, K. Yao, F. Ding, Y. Xu, X. Xin, X. Li, A. K.-Y. Jen, Adv. Funct. Mater., 2015, 25, 4889.

APPENDIX A

NMR DATA

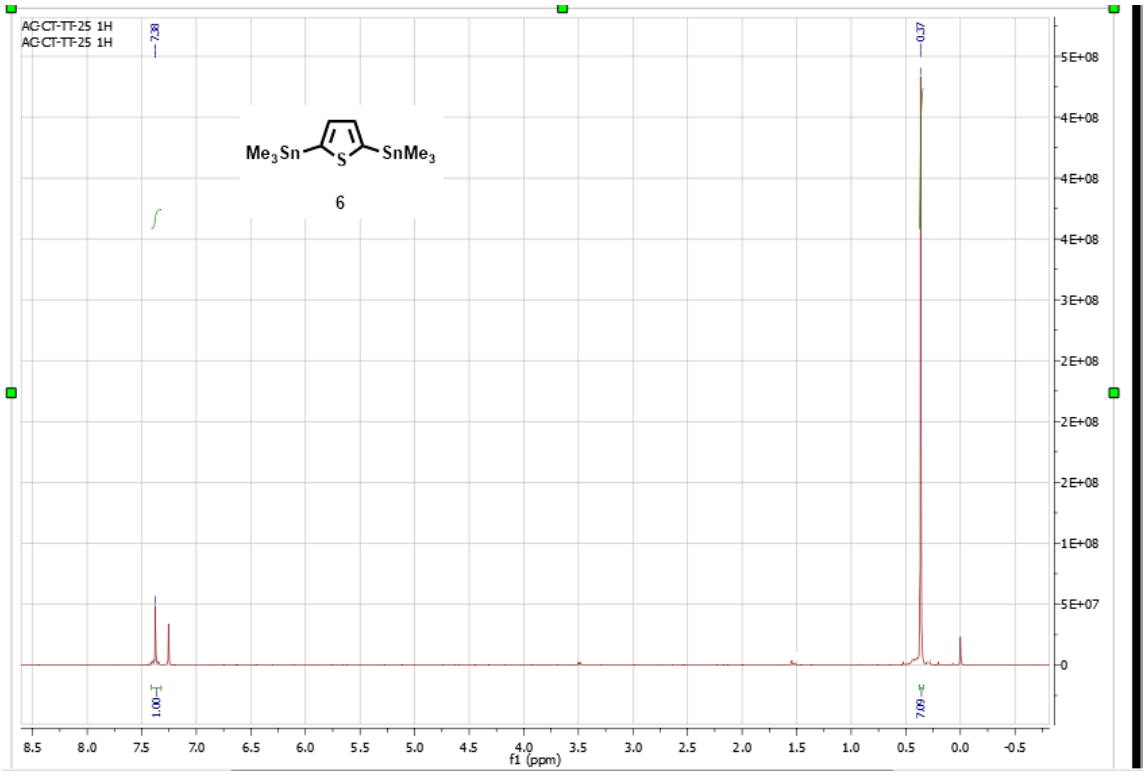

Figure 38. [1]H NMR result of 2,5-bis(trimethylstannyl)thiophene (6)

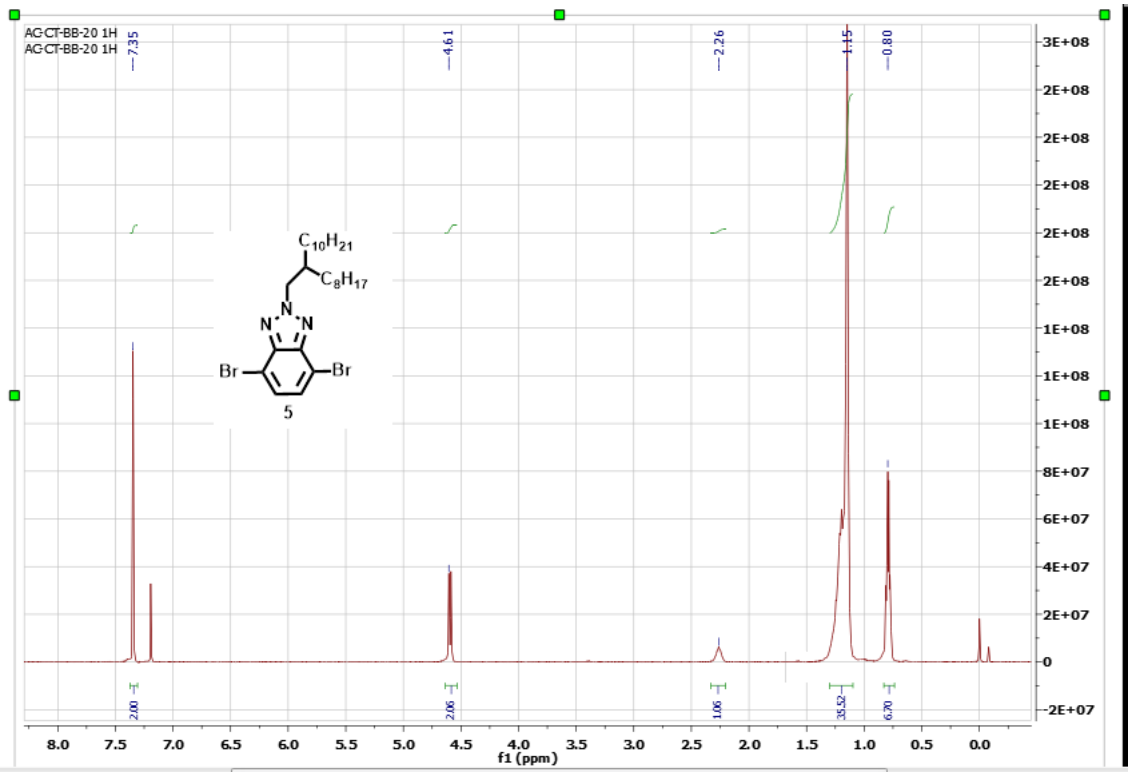

Figure 39. ^{1}H NMR result of 4,7-dibromo-2-(2-octyldodecyl)-2H-benzo[d][1,2,3]triazole

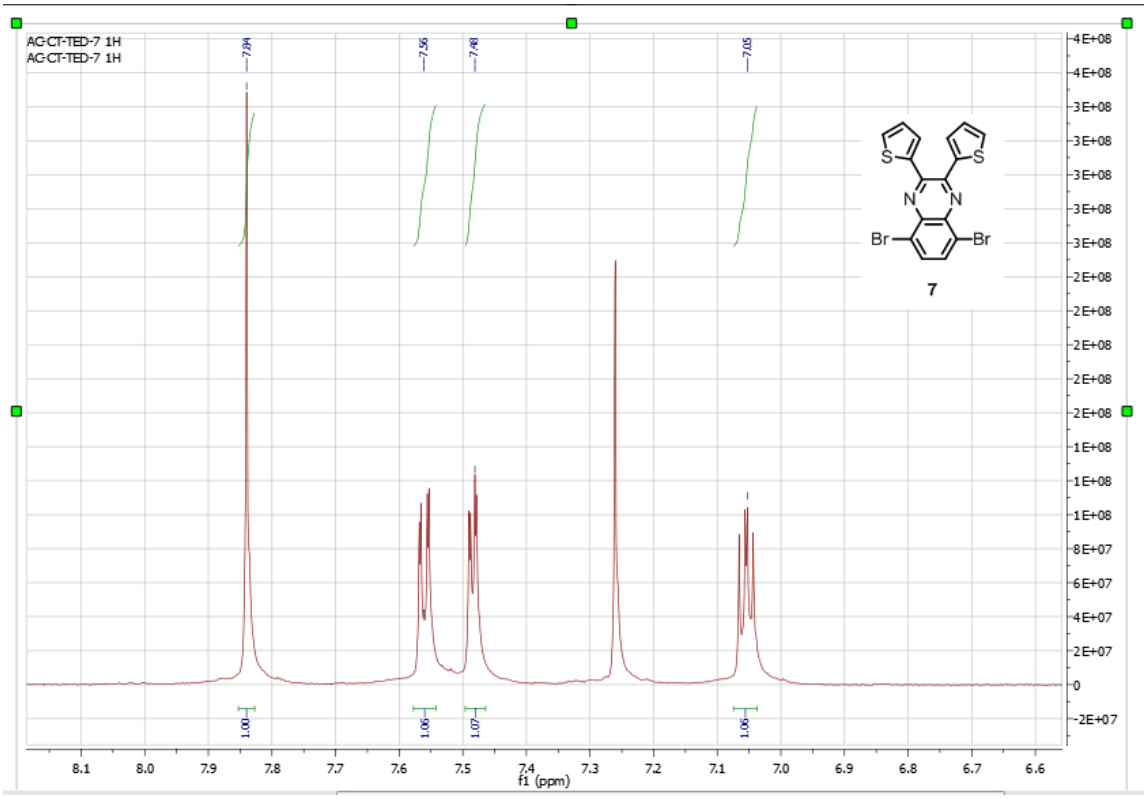

Figure 40. ^{1}H NMR result of 5,8-dibromo-2,3-di(thiophen-2-yl)quinoxaline

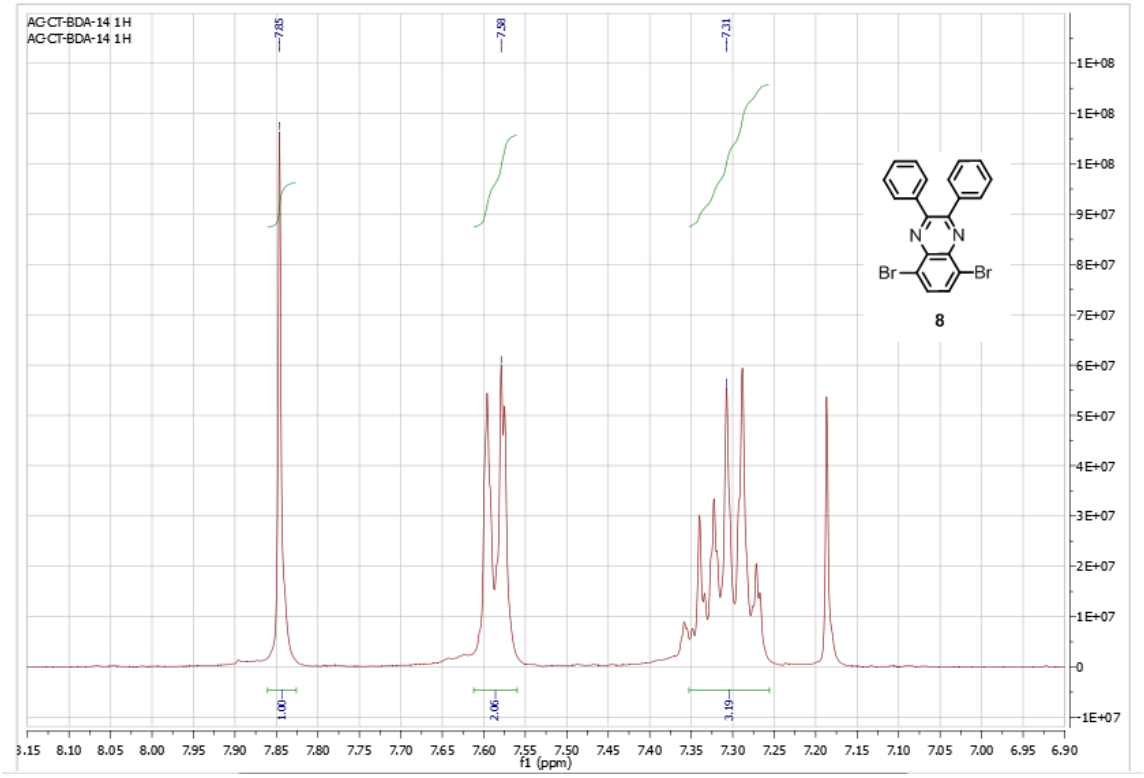

Figure 41. [1]H NMR result of 5,8-dibromo-2,3-diphenylquinoxaline

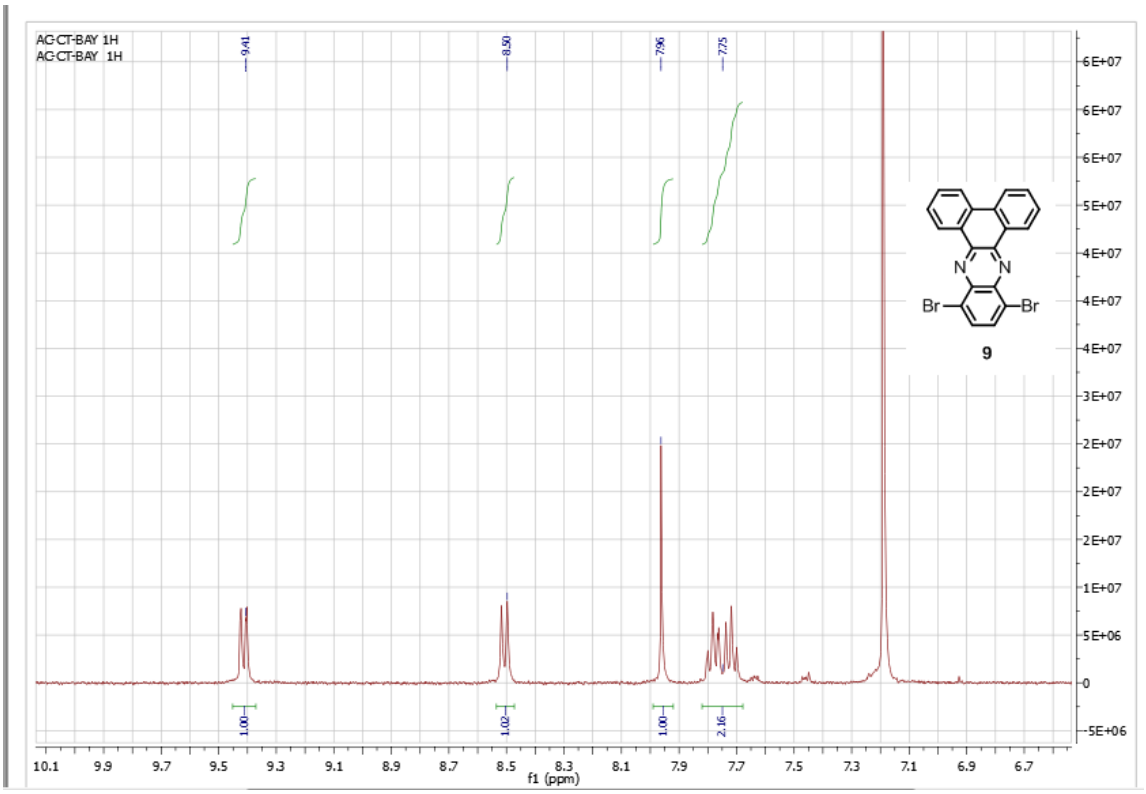

Figure 42. ^{1}H NMR result of 10,13-dibromodibenzo[a,c]phenazine

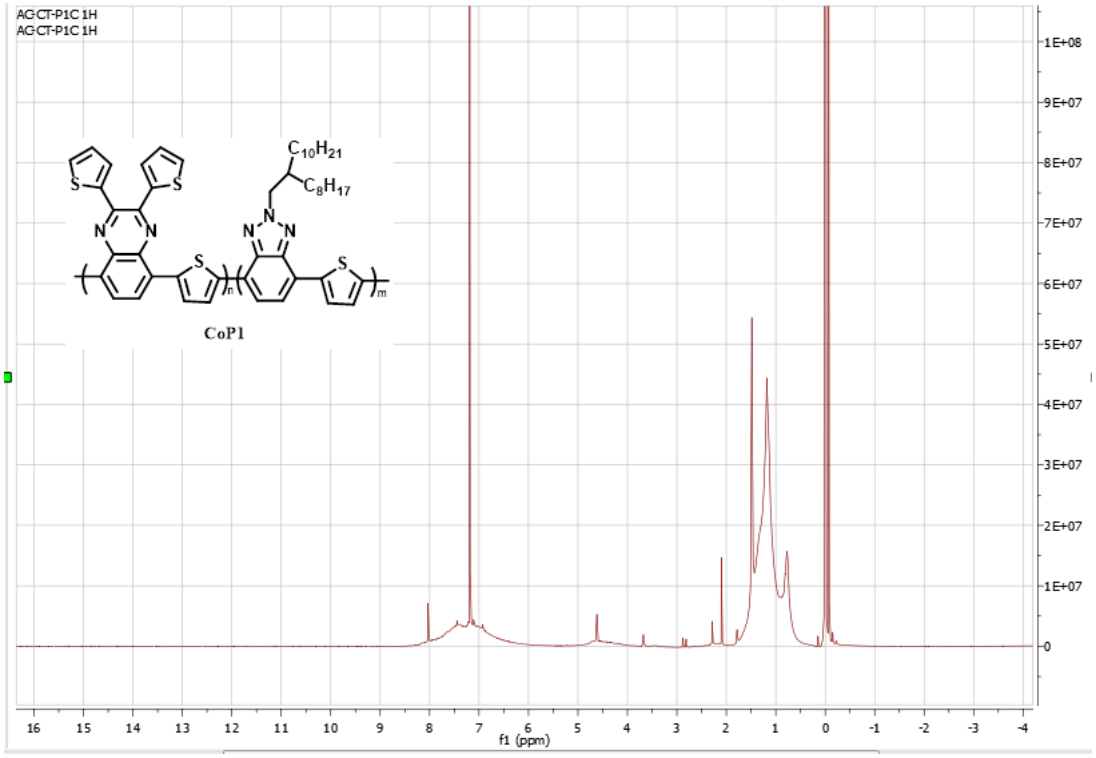

Figure 43. ^{1}H NMR result of **CoP1**

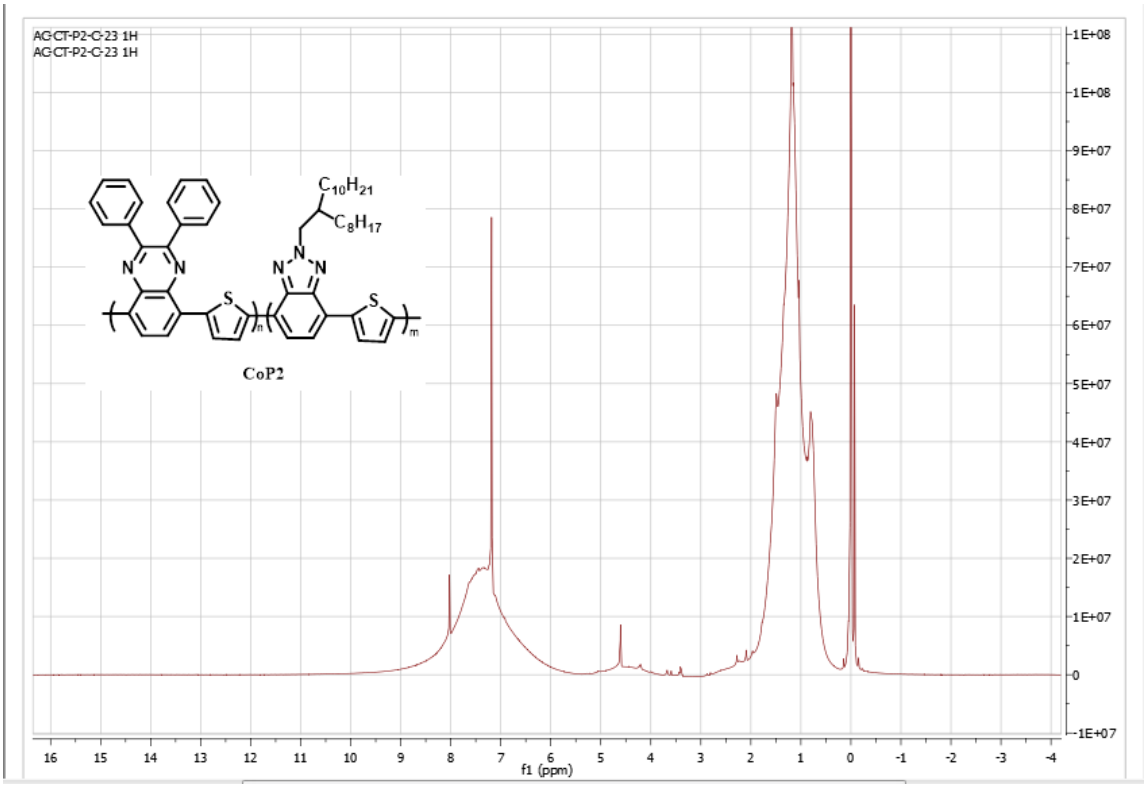

Figure 44. ^{1}H NMR result of **CoP2**

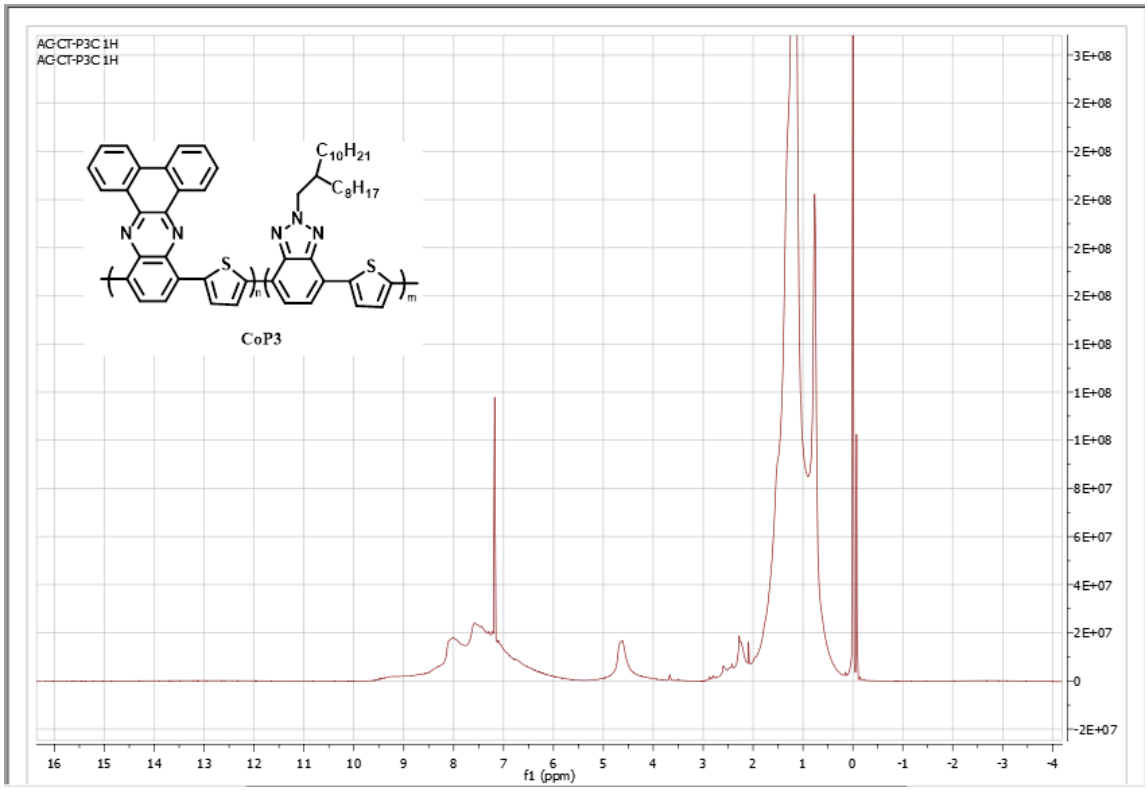

Figure 45. ^{1}H NMR result of **CoP3**

THERMAL ANALYSES RESULTS

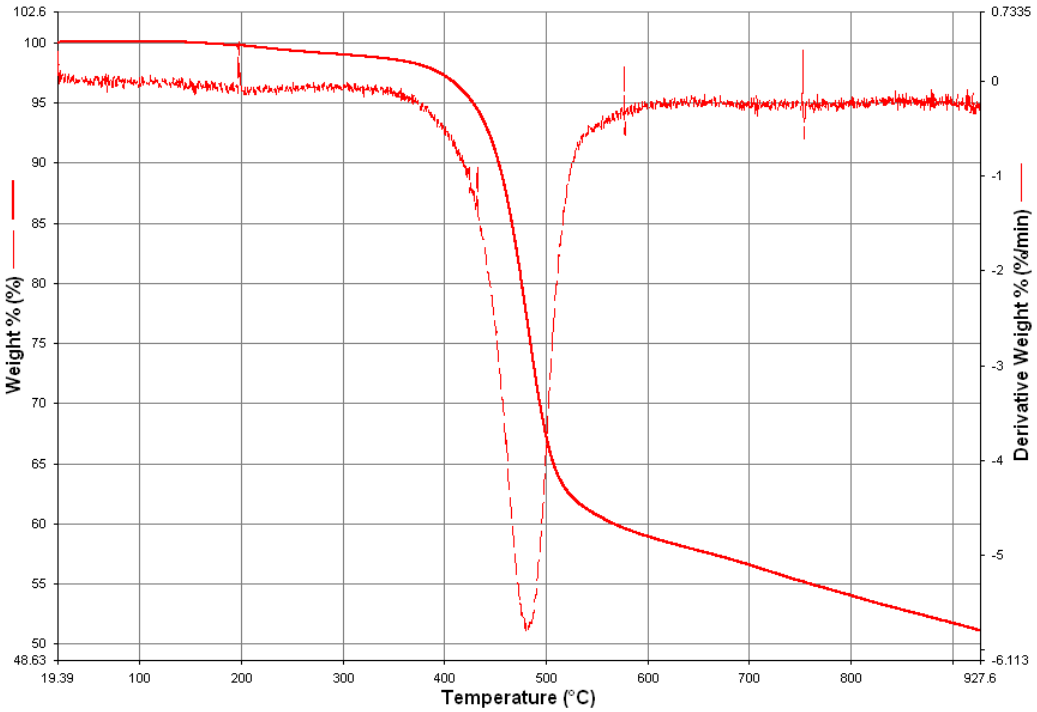

Figure 46. TGA curve of **CoP1**

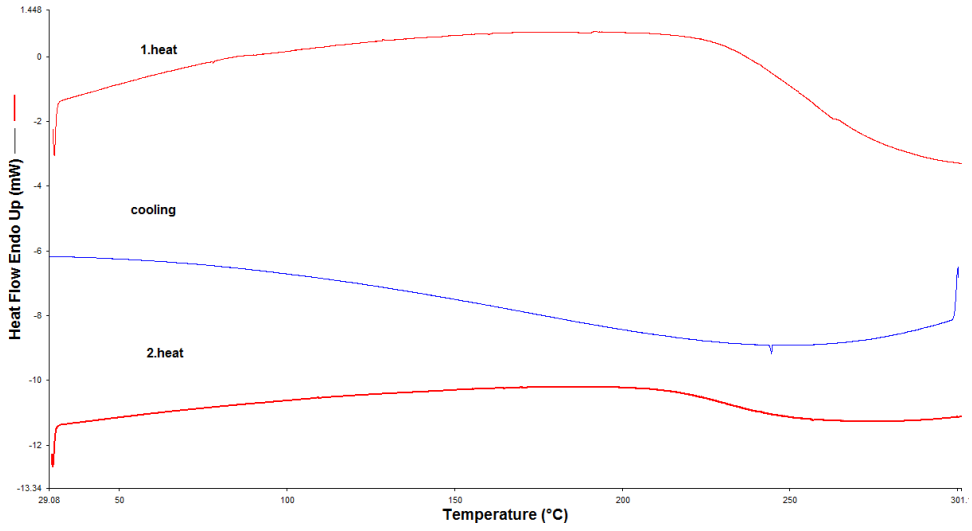

Figure 47. DSC thermogram of **CoP1**

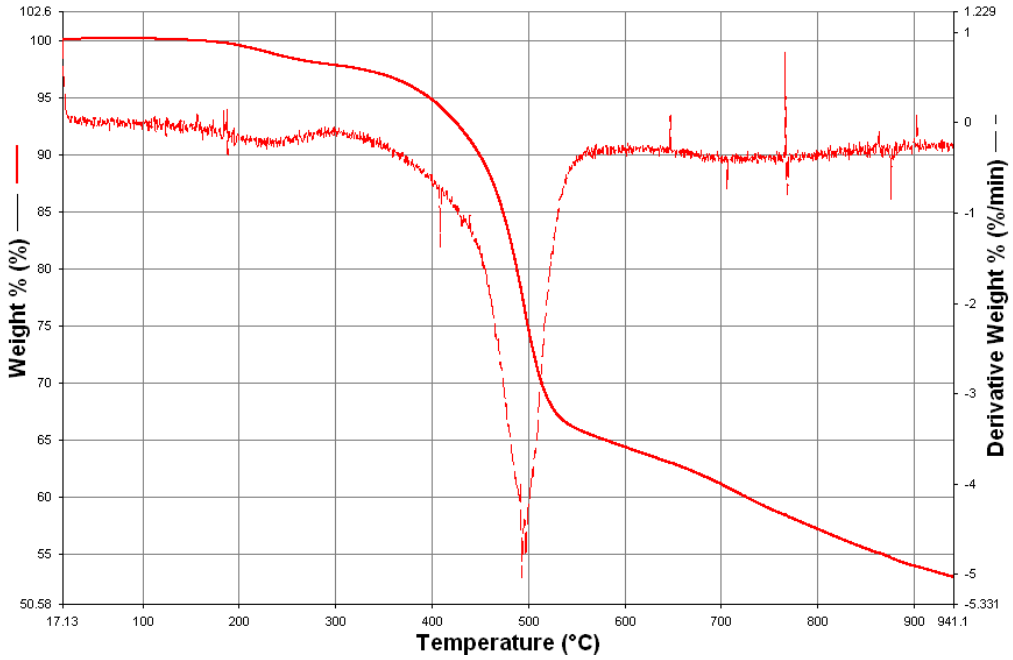

Figure 48. TGA curve of **CoP2**

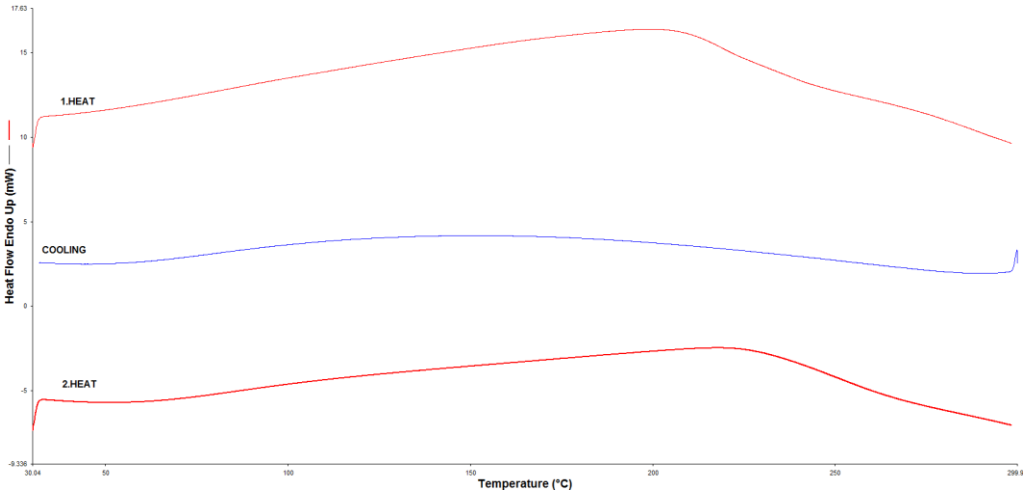

Figure 49. DSC thermogram of **CoP2**

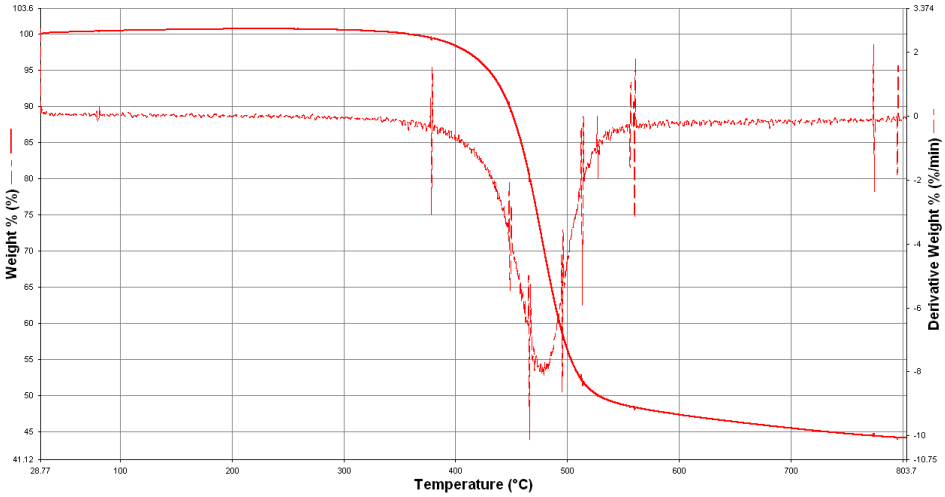

Figure 50. TGA curve of **CoP3**

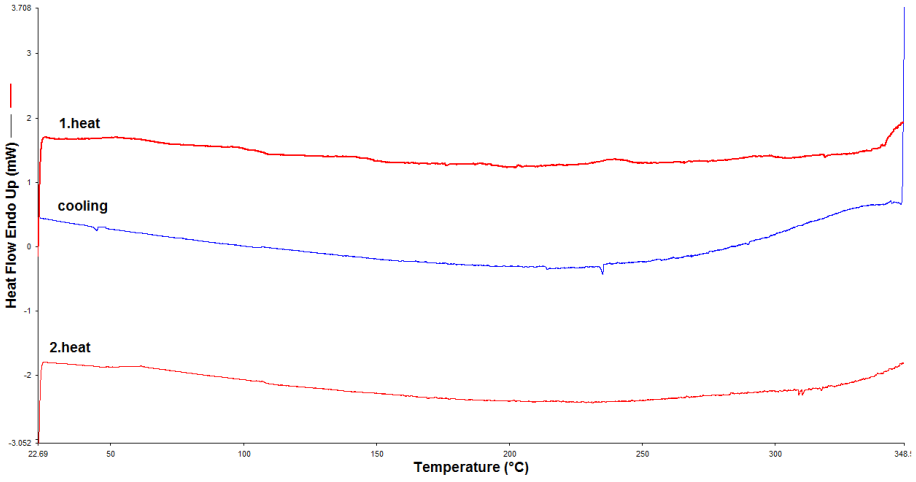

Figure 51. DSC thermogram of **CoP3**